Across-arc versus along-arc Sr-Nd-Pb isotope variations in the Ecuadorian volcanic arc

Marie-Anne Ancellin, Pablo Samaniego, Ivan Vlastélic, François Nauret, Adbelmouhcine Gannoun, Silvana Hidalgo

AGU PUBLICATIONS

Geochemistry, Geophysics, Geosystems

RESEARCH ARTICLE
10.1002/2016GC006679

Across-arc versus along-arc Sr-Nd-Pb isotope variations in the Ecuadorian volcanic arc

Marie-Anne Ancellin[1], Pablo Samaniego[1], Ivan Vlastélic[1], François Nauret[1], Adbelmouhcine Gannoun[1], and Silvana Hidalgo[2]

[1]Université Clermont Auvergne, CNRS, IRD, OPGC, Laboratoire Magmas et Volcans, Clermont-Ferrand, France, [2]Instituto Geofísico, Escuela Politécnica Nacional, Quito, Ecuador

Key Points:
- Subduction of a younger oceanic crust in the northern arc promotes slab melting
- Southward increase of crustal contamination along the front arc (from 3% to 14%)
- The slab structure (Grijalva Fracture Zone, age) and shape (flexure along the Grijalva Fracture Zone) influences magmatism

Supporting Information:
- Supporting Information S1
- Data Set S1

Correspondence to:
Marie-Anne Ancellin
m.a.ancellin@opgc.univ-bpclermont.fr

Citation:
Ancellin, M.-A., P. Samaniego, I. Vlastélic, F. Nauret, A. Gannoun, and S. Hidalgo (2017), Across-arc versus along-arc Sr-Nd-Pb isotope variations in the Ecuadorian volcanic arc, *Geochem. Geophys. Geosyst.*, *18*, 1163–1188, doi:10.1002/2016GC006679.

Received 10 OCT 2016
Accepted 20 FEB 2017
Accepted article online 27 FEB 2017
Published online 24 MAR 2017

Abstract Previous studies of the Ecuadorian arc (1°N–2°S) have revealed across-arc geochemical trends that are consistent with a decrease in mantle melting and slab dehydration away from the trench. The aim of this work is to evaluate how these processes vary along the arc in response to small-scale changes in the age of the subducted plate, subduction angle, and continental crustal basement. We use an extensive database of 1437 samples containing 71 new analyses, of major and trace elements as well as Sr-Nd-Pb isotopes from Ecuadorian and South Colombian volcanic centers. Large geochemical variations are found to occur along the Ecuadorian arc, in particular along the front arc, which encompasses 99% and 71% of the total variations in $^{206}Pb/^{204}Pb$ and $^{87}Sr/^{86}Sr$ ratios of Quaternary Ecuadorian volcanics, respectively. The front arc volcanoes also show two major latitudinal trends: (1) the southward increase of $^{207}Pb/^{204}Pb$ and decrease of $^{143}Nd/^{144}Nd$ reflect more extensive crustal contamination of magma in the southern part (up to 14%); and (2) the increase of $^{206}Pb/^{204}Pb$ and decrease of Ba/Th away from ~0.5°S result from the changing nature of metasomatism in the subarc mantle wedge with the aqueous fluid/siliceous slab melt ratio decreasing away from 0.5°S. Subduction of a younger and warmer oceanic crust in the Northern part of the arc might promote slab melting. Conversely, the subduction of a colder oceanic crust south of the Grijalva Fracture Zone and higher crustal assimilation lead to the reduction of slab contribution in southern part of the arc.

1. Introduction

It is widely accepted that magmas of subduction zones are generated in the mantle wedge as a result of dehydration or melting process in the subducting slab. Released fluids or melts rise through the mantle wedge, modifying its composition by metasomatism and reducing its solidus temperature. Primitive arc magmas are almost never sampled in continental arc settings due to extensive crustal processing as magma rises. Thus, tracing the contribution of the potential sources in arc magma genesis (subducted slab, mantle wedge, and complex arc crust) is a challenging task. In addition, deep-seated magmatic processes impact trace element recycling at subduction zones [*Spandler and Pirard*, 2013] and formation of continental crust [*Martin et al*., 2014; *Gazel et al*., 2015].

In this paper, we examine magma source variations in the Ecuadorian arc, located in the Northern Andean Volcanic Zone (NVZ). Most studies on magma sources in this arc segment focused on geochemical variations associated with the distance from the trench [*Barragan et al*., 1998; *Bourdon et al*., 2003; *Bryant et al*., 2006; *Le Voyer et al*., 2008; *Chiaradia et al*., 2009; *Hidalgo et al*., 2012], which were carried out along East-West transects at ~0–0.5°S. All the studies noted a marked across-arc geochemical zonation, which is expressed by an increase in incompatible element contents (e.g., K, Ba, Nb, Rb, La, Pb, Th) away from the trench, while ratios of trace elements that are more versus less fluid-mobile decrease (e.g., Ba/Th, Ba/La, Ba/Nb, Pb/Th, Li/Th, B/Be). These features were interpreted as a decrease in the degree of mantle partial melting induced by a reduction of slab fluids input into the mantle further away from the trench [*Barragan et al*., 1998; *Bourdon et al*., 2003; *Le Voyer et al*., 2008; *Hidalgo et al*., 2012]. An additional feature concerns the Sr-Nd isotope zonation, which is ascribed to the upper crustal interaction of an oceanic-like basement (forming the Western Cordillera) or a continental basement (below the Eastern Cordillera) with magmas by a process of crustal melting and/or assimilation [*Bryant et al*., 2006; *Chiaradia et al*., 2009; *Hidalgo et al*., 2012]. Up to 14% upper crustal assimilation is estimated for volcanoes of both Cordilleras.

A second geochemical characteristic of the Ecuadorian arc is the occurrence of the so-called "adakitic" lavas [e.g., *Defant and Drummond*, 1990]. This term was defined to describe andesites and dacites with high concentrations of Al_2O_3 (>15 wt %) and Na_2O (3.5–7.5 wt %), low concentrations of heavy REE and Y (Y < 18 ppm, Yb < 2 ppm), high concentration in Sr (> 400 ppm) resulting in extreme enrichment in LREE over HREE (La/Yb > 9) and high Sr/Y ratios (>50). However, this term has often been used loosely, based on the assumption that all rocks displaying these characteristics are derived from subducted slab melting in the eclogite facies. We choose not to use this term to clearly separate the geochemical composition of rocks and their formation processes. Several interpretations for this characteristic in Ecuadorian lavas have been raised: partial melting of the slab and its subsequent interactions in the mantle wedge [*Bourdon et al*., 2003; *Samaniego et al*., 2005; *Hidalgo et al*., 2012], crustal melting and/or assimilation of the lower crust [*Garrison and Davidson*, 2003; *Garrison et al*., 2006, 2011] and even high-pressure fractionation of garnet and/or amphibole [*Bryant et al*., 2006; *Chiaradia et al*., 2009]. Some authors consider these processes as to be mutually exclusive even though they can all occur during the evolution of arc magmas.

In this paper, we aim to evaluate the relative influence of deep-seated processes taking place in the subducted slab and mantle wedge, and shallower processes occurring in the crust. Our study focused on the scale of the whole arc and relates magma source variations to the geological and geodynamical characteristics of the Quaternary Ecuadorian arc. Previous large scale studies of arcs, including the New Hebrides Central Chain [*Monzier et al*., 1997], the Aleutian arc [*Kelemen et al*., 2003; *Yogodzinski et al*., 2015], the Sangihe arc [*Hanyu et al*., 2012], the Izu-Bonin arc [*Ishizuka et al*., 2007], the Andean Central Volcanic Zone [*Mamani et al*., 2008], the Central American Volcanic Arc [*Heydolph et al*., 2012], and the Andean Southern Volcanic Zone [*Hildreth and Moorbath*, 1988; *Hickey-Vargas et al*., 2016], show that large along-arc geochemical variations are either linked to a lateral change in slab contribution or to the heterogeneity of arc crust. We find significant geochemical variations along the Ecuadorian arc (North-South variations), which show that it is necessary to take all spatial dimensions into account to obtain a complete understanding of how magma sources vary spatially in Ecuador.

2. Geological Setting

The Northern Volcanic Zone (NVZ) of the Andes results from the subduction of the Nazca plate below the South-American lithosphere. Three tectonically distinct ocean floor domains characterize the Nazca plate to the west of Colombia, Ecuador and Northern Peru (Figure 1). In Colombia, between latitudes 7°N and 1°N, the subducted plate is 10–26 Ma old and plunges at roughly 30–35° with an azimuth of N120° [*Pennington*, 1981]. In front, the Colombian volcanic arc is made up of a single row of stratovolcanoes. In southern Ecuador and northern Peru, south of 2°S–3°S, the subducting slab is older (25–30 Ma) and dips at only 10–14°, defining a flat slab segment [*Barazangi and Isacks*, 1976; *Gutscher et al*., 1999], and no active volcanism exists. Between these two domains (i.e., from 1°N to 2°S), the Nazca plate and the overlying Carnegie Ridge impinge upon and subduct beneath mid-northern Ecuador. The Carnegie Ridge is a 200–250 km wide, 2 km high aseismic submarine mountain range that represents the track of the Galapagos hot spot across the Nazca plate. It is constructed upon a relatively young (12–16 Ma) oceanic crust [*Sallarès et al*., 2003]. The current convergence rate of this segment with South America is estimated at 5–6 cm/yr with a dip of around 25° and an azimuth of N83°E [*Guillier et al*., 2001; *Kendrick et al*., 2003]. The Ecuadorian province of the NVZ is characterized by an extensive volcanism with at least 80 volcanic centers of Pleistocene-Holocene age, which are distributed along the Western and Eastern Cordilleras, the Inter-Andean valley and the back-arc region [*Hall et al*., 2008; *Bernard and Andrade*, 2011].

The Ecuadorian Andes consist of two subparallel mountain ranges, the Western and Eastern Cordilleras, which are separated by a tectonic depression, termed the Inter-Andean valley. The active volcanic arc is distributed along and across these structures, including an additional group of volcanoes located to the east, along the sub-Andean Amazonian low lands (Figure 2). Based on gravimetric and seismological studies, the crustal thickness is inferred to be >50 km beneath the active volcanic arc [*Feinenger and Seguin*, 1983; *Prevot et al*., 1996; *Guillier et al*., 2001]. The composition and age of the crustal basement beneath these volcanic alignments varies. The Western Cordillera basement consists of oceanic MORB-like basalts and overlying sedimentary rocks, which were accreted onto the ancient Ecuadorian margin during Late Cretaceous and Cenozoic times [*Hughes and Pilatasig*, 2002; *Luzieux et al*., 2006; *Jaillard et al*., 2008]. In contrast, the Eastern

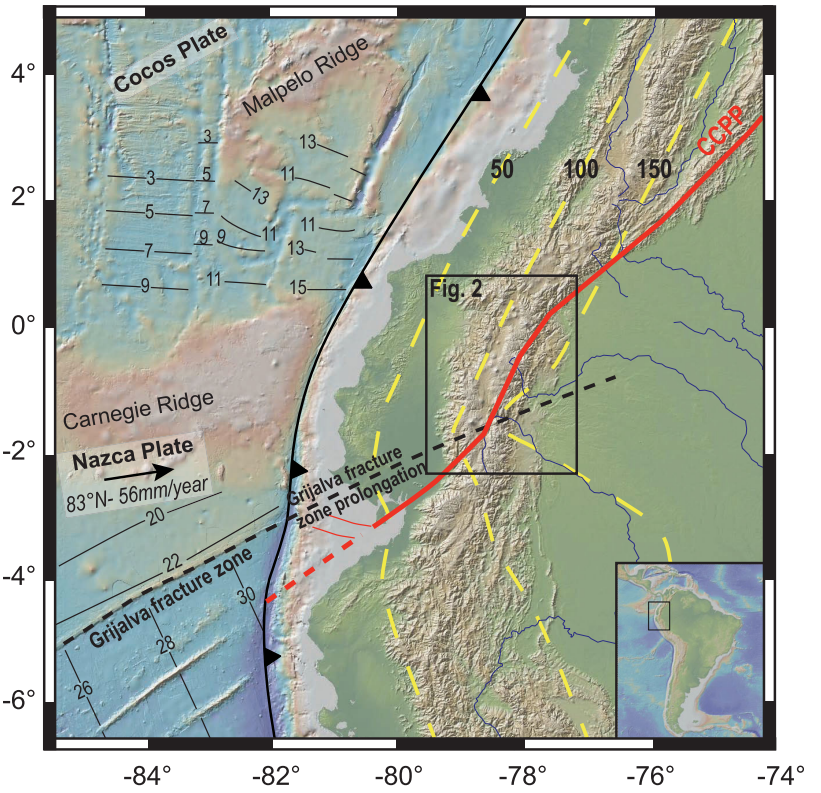

Figure 1. Geological setting of Ecuador (modified from *Yepes et al.* [2016]). CCPP consists of four major transpressive fault systems from NE to SW: Chingual, Cosanga, Pallatanga, and Puñá. Lines on the oceanic floor represent magnetic anomalies with their corresponding ages (modified after *Lonsdale et al.* [2005]). Dashed yellow lines correspond to the slab depth beneath the arc (from *Yepes et al.* [2016]). In the text, the oceanic plate south to the Grijalva Fracture Zone is referred as the southern Nazca plate.

Cordillera basement consists of older continental formations, made up of Palaeozoic to late Mesozoic felsic and mafic igneous and metamorphic rocks [*Aspden and Litherland*, 1992; *Chiaradia et al.*, 2004]. Basement rocks in both cordilleras are overlain by Cenozoic volcanic and volcaniclastic deposits. Lastly, the basement of the Amazonian basin is formed by the Guyanese craton [*Aspden and Litherland*, 1992], which is overlain by Mesozoic to Cenozoic sedimentary sequences [*Baby et al.*, 2004].

In a recent paper, *Yepes et al.* [2016] stress the importance of an additional topographic feature that characterizes the subduction of the Nazca plate: the Grijalva fracture zone which subducts between 2°S and 3°S, in front of the Gulf of Guayaquil (Figure 1). It consists of a 500 m high escarpment separating "young" crust derived from the Galapagos spreading center to the north from "old" crust formed at the East Pacific rise to the south. The difference of up to nine million years in age between the young and old crustal segments is probably associated with a density contrast [cf. *Yepes et al.*, 2016]. As the Grijalva fracture zone is believed to have been subducting for at least the last 3–6 Ma [*Lonsdale*, 2005; *Michaud et al.*, 2009; *Yepes et al.*, 2016], the contact between those two oceanic segments should lie beneath the Andean arc. The presence of both this escarpment and the Carnegie Ridge will have a strong influence not only on the morphology of the subducted slab but also on the thermal regime of the slab-mantle system. It is widely accepted [*Peacock et al.*, 1994; *Syracuse et al.*, 2010] that the age of the subducted slab coupled with the presence (or not) of asperities in the slab are the main parameters controlling the geothermal regime at the slab-mantle interface.

3. Sampling Strategy and Analytical Methods

Over the last two decades an extensive geochemical database has been developed for Quaternary Ecuadorian lavas through a French-Ecuadorian cooperative program between the Institut de Recherche pour le

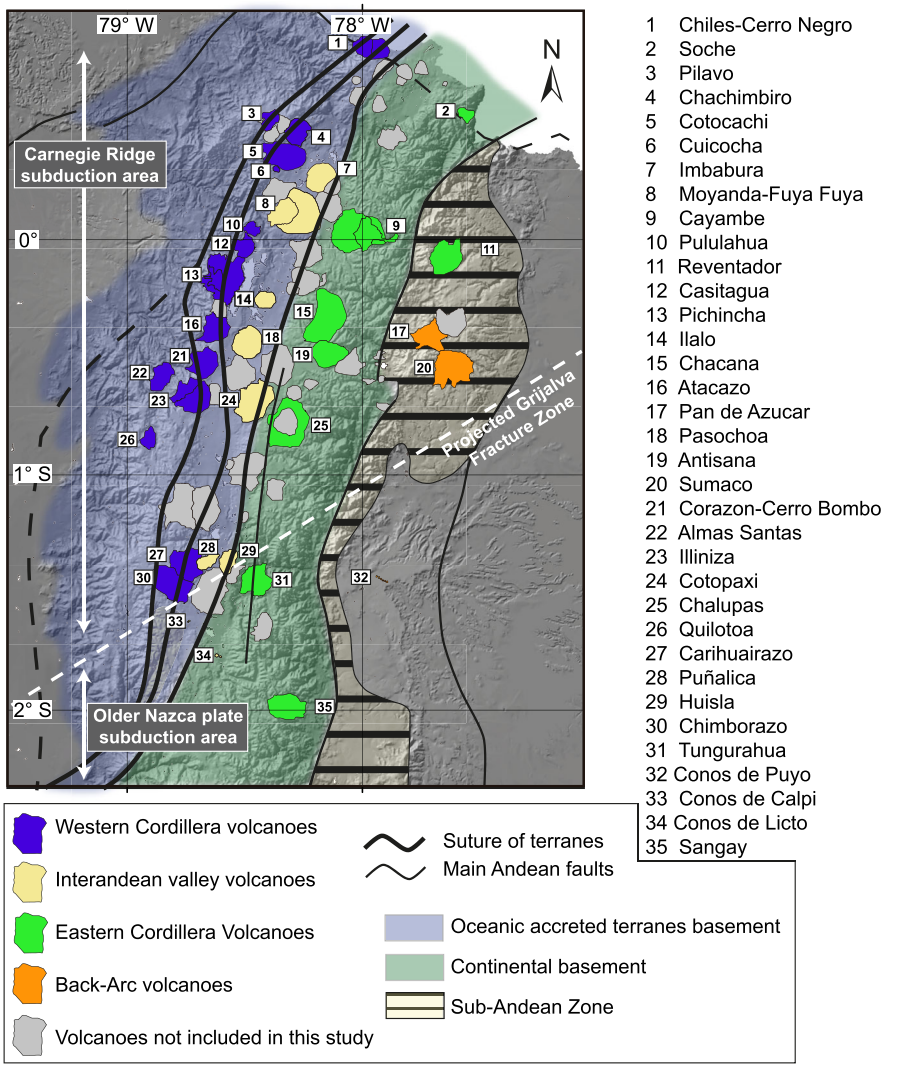

Figure 2. Schematic map of the main geological zones in Ecuador (modified from *Jaillard et al.* [2008]). Volcanic centers are displayed and sorted according to their geographical location (Western Cordillera, Inter-Andean Valley, Eastern Cordillera, and back arc). Basement compositions are separated into oceanic (blue) and continental (green), although detailed maps show a degree of interleaving. Projection of the Grijalva Fracture Zone, separating the younger Nazca plate carrying the Carnegie Ridge to the North and the older Nazca plate to the South, is displayed.

Développement (IRD) and the Instituto Geofísico of the Escuela Politécnica Nacional (IG-EPN). A large part of these data have been published in two regional-oriented papers that discussed the trace element [*Schiano et al.*, 2010] and Sr-Nd-O isotopic variations [*Hidalgo et al.*, 2012] of the Ecuadorian volcanic arc. Additional data have been published by our group and other authors, in papers dealing with several large Ecuadorian volcanoes such as Sangay [*Monzier et al.*, 1999], Antisana [*Bourdon et al.*, 2002b], Cayambe [*Samaniego et al.*, 2005], Illinizas [*Hidalgo et al.*, 2007]; Puyo and Pan de Azucar [*Hoffer et al.*, 2008], Reventador [*Samaniego et al.*, 2008], Mojanda-Fuya Fuya [*Robin et al.*, 2009], Pichincha [*Bourdon et al.*, 2002a; *Robin et al.*, 2008; *Samaniego et al.*, 2010], Cotopaxi [*Garrison et al.*, 2006, 2011], Pilavo [*Chiaradia et al.*, 2011], Chimborazo [*Samaniego et al.*, 2012], and Tungurahua [*Samaniego et al.*, 2011]. Some data were also published in regional studies such as those of *Barragan et al.* [1998], *Bourdon et al.* [2003], *Bryant et al.* [2006], and *Chiaradia et al.* [2009]. Additional data from *Droux and Delaloye* [1996] and the IRD/IG-EPN unpublished database were also used to include the Southern Colombian volcanoes (Azufral de Tuquerres, Cumbal, Doña Juana, and Galeras) in this regional study. On the basis of this extensive database (1437 samples), which covers the entire volcanic arc, we selected 71 samples from 33 volcanoes located in the Western and Eastern Cordilleras, the Inter-Andean valley, and the back-arc region. We chose samples to fill local gaps in

data and improve our view of the geographical distribution of volcano signatures on the scale of Ecuador as a whole. New data are provided in the supporting information.

3.1. Major and Trace Element Chemistry

Most major and trace element analyses were performed at the Laboratoire Domaines Océaniques, Université de Bretagne Occidentale (Brest, France). For major elements, agate-ground powders were dissolved in HNO_3 and HF and then measured by Inductively Coupled Plasma-Atomic Emission Spectroscopy (ICP-AES), following the method described by *Cotten et al*. [1995]. Trace element compositions of a selected group of samples (57) analyzed for Sr-Nd-Pb isotopes were reanalyzed following the method of *Barrat et al*. [1996]. For this subgroup, agate-ground powders were also dissolved in HNO_3 and HF and spiked with a thulium solution used as the internal standard. Samples were analyzed by quadrupole Inductively Coupled Plasma Mass Spectrometer (ICP-MS) along with three rock standards (BHVO-2 for calibration and BCR2 and Bir 1 as blind standards to measure the results' reliability). Relative standard deviations were 1% for SiO_2 and $\leq$2% for the other major elements. For trace elements, the relative standard deviation was $\leq$5%.

3.2. Pb, Sr, and Nd Isotope Analysis

All samples were leached with 6 *N* HCl in order to eliminate potential dust contamination in the crushing room. Samples were placed for 15 min in an ultrasonic bath, and after about 45 min of decantation, HCl was removed with a pipette. The powder was rinsed with 18.2 MΩ water following the same procedure as for HCl. About 100 mg of powdered samples were dissolved in a solution composed of 2 mL of concentrated HF and 1 mL of concentrated HNO_3 at 90°C for 48 h and then evaporated to dryness at 90°C. Each sample batch included a standard and a blank. NBS981 was processed as a sample to evaluate potential isotopic bias during Pb separation. Lead blanks were determined by isotopic dilution using the NBS983 spike: they ranged from 8 to 18 pg, with one value at 105 pg. In order to minimize fluoride precipitates, 15 drops of concentrated HNO_3 were placed on the deposit and evaporated at 90°C. Then, 15 drops of concentrated HBr were put in the beaker and evaporated to dryness. Indeed, this is necessary to convert all the lead present in bromide form, suitable for our chemical separation scheme. Samples were centrifugated and loaded on 100 μL teflon columns filled with an anionic resin (Bio-Rad AG1-X8 resin 100–200 mesh) for lead purification [*Vlastelic et al*., 2013]. The separation process was carried out twice consecutively. The fraction containing Nd and Sr was recovered for further purification. Insoluble fluorides were dissolved and analyzed by ICP-MS (Agilent 7500, Laboratoire Magmas et Volcans, Clemont-Ferrand) in order to estimate the amount of Pb, Nd, and Sr left behind. Depending on the sample, up to 89% of Nd was trapped in insoluble fluorides. Thus, for some samples, a new dissolution was performed for Nd and Sr separations.

Pb isotopic composition was analyzed with a MC-ICP-MS Neptune Plus, coupled to an Aridus II desolvating nebulizer system (Laboratoire Magmas et Volcans, Clermont-Ferrand). Samples were diluted in a solution of HNO_3 0.05 *N* spiked with Thallium NBS997 so that the solution has 20 ppb Pb and 4 ppb Tl. Thallium is used to correct isotope ratios for instrumental mass bias and drift. Repeated analysis of the NBS981 standard yielded an error of approximately 50 ppm/a.m.u. over the sessions. Tl-normalized ratios were renormalized to the NBS981 value recommended by *Todt et al*. [1996] ($^{206}Pb/^{204}Pb = 16.9356$, $^{207}Pb/^{204}Pb = 15.4891$, $^{206}Pb/^{204}Pb = 36.7006$).

For Sr and Nd separation, samples were processed through four columns following the method of *Pin et al*. [1994] and *Pin and Santos Zalduegui* [1997]. First, AG50 X8 removed Fe ions, which could reduce efficiency of TRU spec columns. After evaporation and dissolution in HNO_3 2 *M*, a coupled passage on Sr spec and TRU spec was used to separate Sr and rare earth elements. Lastly, Nd was isolated with LN spec columns. Strontium and Neodymium isotopic measurements were performed by TIMS (TRITON, Laboratoire Magmas et Volcans, Clermont-Ferrand) and MC-ICP-MS (Neptune plus coupled to an Aridus II desolvating nebulizer system, Laboratoire Magmas et Volcans, Clermont-Ferrand), respectively. $^{87}Sr/^{86}Sr$ and $^{143}Nd/^{144}Nd$ ratios were normalized to $^{86}Sr/^{88}Sr = 0.1194$ and $^{146}Nd/^{144}Nd = 0.7219$, respectively. Sr and Nd isotopic ratios are given relative to $^{87}Sr/^{86}Sr = 0.710230 \pm 11$ (2σ) for NBS SRM987 and $^{143}Nd/^{144}Nd = 0.512115 \pm 16$ (2σ) for JNdi-1. Total procedural blanks were lower than 1 ng for both Sr and Nd.

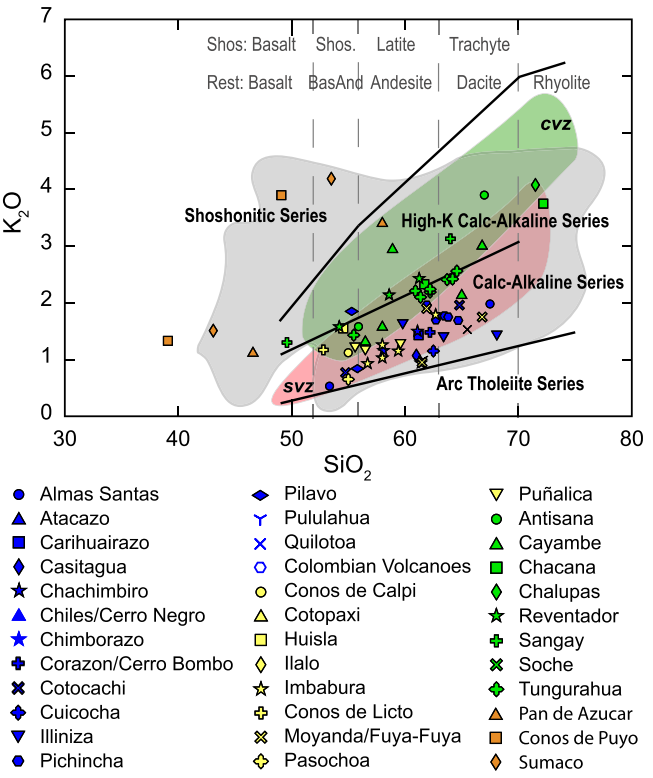

Figure 3. SiO_2 versus K_2O diagram of *Peccerillo and Taylor* [1976] classifying arc rock types. Samples from the literature are represented by the gray-shaded area [*Barragan et al.*, 1998; *Bourdon et al.*, 2002a, 2002b; *Bourdon et al.*, 2003; *Samaniego et al.*, 2005; *Bryant et al.*, 2006; *Hidalgo et al.*, 2007; *Robin et al.*, 2008; *Hoffer et al.*, 2008; *Chiaradia et al.*, 2009; *Schiano et al.*, 2010; *Samaniego et al.*, 2010; *Samaniego et al.*, 2011; *Chiaradia et al.*, 2011; *Garrison et al.*, 2011; *Hidalgo et al.*, 2012] and samples from this study are displayed (see supporting information).Volcano geological setting is color coded according to: blue = Western Cordillera (WC), Yellow = Inter-Andean Valley (IV), Green = Eastern Cordillera (EC), Orange = Back-Arc (BA). Arc zonation is visible as alkaline content at given SiO_2 increases away from the trench. Composition of other Andean volcanic zones are displayed, the Central Volcanic Zone (CVZ) by the green shaded area [*Davidson and de Silva*, 1992; *Feeley and Davidson*, 1994; *Delacour et al.*, 2007; *Hora et al.*, 2007; *Mamani et al.*, 2008, 2010; *Sørensen and Holm*, 2008] and the Southern Volcanic Zone (SVZ) by the red shaded area [*Hickey-Vargas et al.*, 2016].

4. Results

4.1. Major and Trace Elements

Whole-rock analyses of Ecuadorian volcanic rocks define a broad medium-K to high-K calc-alkaline magmatic trend (Figure 3). Most samples are basaltic andesites to dacites (52–70 wt % SiO_2) while some basalts and rhyolites can be found amongst back-arc and Eastern Cordillera samples, respectively. Back-arc samples differ from the others as they plot along the alkaline trend and display shoshonitic compositions. A key feature of Ecuadorian magmas is that for a given silica content, there is a large diversity of K_2O content, from low concentrations (0.5 wt %) along the Western Cordillera to higher values in the back arc (3–4 wt %). This characteristic is highlighted in Figure 3, where Ecuadorian samples are plotted together with the variation fields of the Central and Southern Volcanic Zones of the Andes [*Mamani et al.*, 2010; *Hickey-Vargas et al.*, 2016] which define narrow calc-alkaline trends.

Our database confirms the across-arc geochemical zonation observed by several authors [*Barragan et al.*, 1998; *Bourdon et al.*, 2003; *Bryant et al.*, 2006; *Le Voyer et al.*, 2008; *Chiaradia et al.*, 2009; *Hidalgo et al.*, 2012]. K_2O and most incompatible elements contents (e.g., Ba, Nb, Pb, Th, Be, Y, Rb, Sr, Zr, all REE) increase with the distance from trench, whereas ratios of fluid-mobile to fluid-immobile ratios decrease (e.g., Ba/Th, Ba/La, Ba/Nb, Pb/Th, Pb/Nb, Li/Th, Li/Nb, Li/La) (Figure 4).

Figure 4 shows along-arc trace element variations. Note that the trends described are observed for both the whole data set and the selected subset of samples with Mg-numbers higher than 50. There is a decrease in the minimum content of incompatible elements toward 0.5°S (e.g., Be, Ba, Th, Pb, La, Yb, Y) for the edifices located on the oceanic basement (those of the Western Cordillera and some volcanoes of the Inter-Andean valley, hereafter called the frontal part of the arc). The incompatible element minimum values tend to increase away from this latitude (Figures 4a and 4b). A similar trend is observed for La (and LREE; not shown) in volcanoes located on the continental basement (those of the Eastern Cordillera and some volcanoes of the Inter-Andean valley, hereafter called main arc). This feature is correlated with maximum values in most incompatible trace elements (e.g., Rb, Pb, Th) in the main arc. In addition, back-arc volcanics have highly variable incompatible element contents. Sumaco volcano is the most enriched back-arc volcano for many incompatible elements (e.g., REE, Th, Nb, Pb) and is located at ~0.5°S. Hence, the maximum contents of most incompatible elements in the back-arc area are also found at ~0.5°S. Thus, volcanoes situated around 0.5°S display the largest range of incompatible element content.

Fluid-mobile elements (e.g., Ba, Pb, Li, Cs) are enriched with respect to fluid-immobile elements (e.g., Th, Nb, La) in the frontal part of the Ecuadorian arc, as pointed out above. It is noteworthy that fluid-mobile to

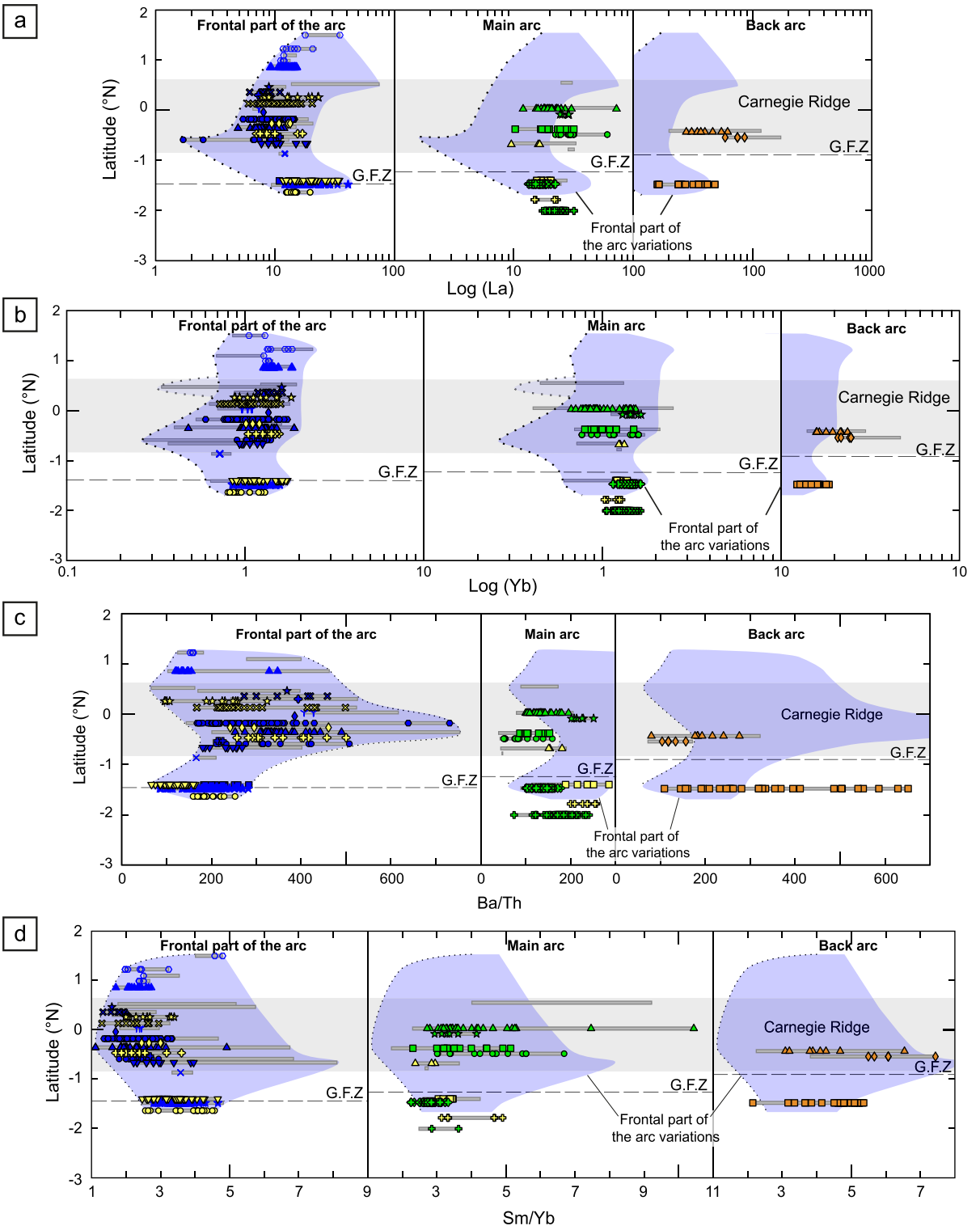

Figure 4. Trace element content and ratio evolutions with latitude. Symbols correspond to samples having Mg# > 50 (legend as for Figure 3), grouped according to basement type: from left to right, edifices located on oceanic crust, continental crust and sub-Andean zone. The blue-shaded area corresponds to geochemical variations in the frontal part of the arc (volcanoes located on the oceanic basement) and the gray field marks the supposed position of the Carnegie Ridge beneath the Ecuadorian arc. The dashed line corresponds to the supposed position of the Grijalva Fracture Zone (GFZ) beneath the arc. (a) log(La) versus latitude (similar trends are also observed for Ba, LREE, and MREE); (b) log(Yb) versus latitude variations (similar trends are also observed for Th, Be, Nb, and Y); (c) Ba/Th versus latitude variations (similar trends are also observed for other "fluid-mobile" versus "fluid-immobile" elements (Pb, Cs, Li, Ba, over Th, Nb, La)); (d) Sm/Yb versus latitude variations (similar trends are also observed for La/Yb). For each volcano, primitive samples with Mg# > 50 (symbols) and unfiltered data (gray bars) are shown. Thus, the trends observed are only slightly affected by differentiation. Trace element data correspond to those of the literature as well as new analyses included in the supporting information. This figure includes IRD-IGEPN data for Chiles-Cerro Negro, Carihuairazo-Puñalica, and Huisla volcanoes given in personal com.

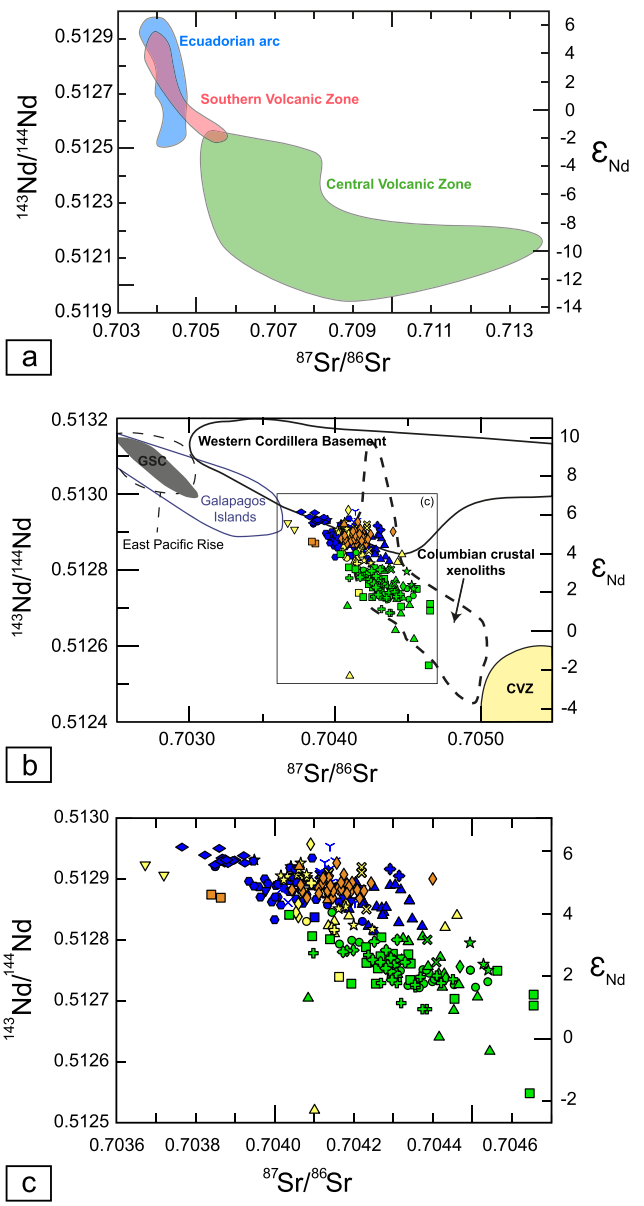

Figure 5. Sr-Nd isotopic compositions of Ecuadorian volcanic products. (a) Compositional fields of Ecuadorian products (data are from the literature—references Figure 3—and new data from this study (supporting information), Central Volcanic Zone (SVZ) and Southern Volcanic Zone (SVZ). (b and c) Sr-Nd isotopic composition of our data set, compositional fields are taken from [*Hidalgo et al*., 2012]; GSC = Galapagos Spreading Center. ε_{Nd} was calculated with a reference chondritic value of $^{143}Nd/^{144}Nd = 0.512638$. Legend as in Figure 3.

fluid-immobile element ratios are high in the northern part of the frontal arc (around 0°S–0.5°S) but are similar to Eastern Cordillera values in its southern part (below 1°S) (Figure 4c). Along the frontal part of the arc, fluid-mobile to fluid-immobile element ratios are clearly more variable, and generally higher at ~0°S–0.5°S latitude.

The decrease of incompatible element minimum content toward 0.5°S is also observed for Sm/Yb ratios in the frontal part of the arc (Figure 4d, also seen with La/Yb). Sm/Yb ratios are more variable and generally higher between 0.5°N and 1°S in the frontal part of the arc and in the northernmost volcanoes located on the continental basement (Soche and Cayambe). In the back-arc area, fractionation between Sm and Yb is maximal in Sumaco samples.

4.2. Sr-Nd Isotopes

On the scale of the Andean arc, Ecuadorian samples resemble those of the Southern Volcanic Zone, although some samples from the SVZ display higher $^{87}Sr/^{86}Sr$ values (Figure 5a). In contrast, the Ecuadorian magmas show less radiogenic Sr and more radiogenic Nd signatures than those of the Andean Central Volcanic Zone (whose maximum $^{87}Sr/^{86}Sr$ is 0.712). Figures 5b and 5c show isotopic data for Ecuador, including both new analyses and published data. The data define a negative correlation on the $^{143}Nd/^{144}Nd$ versus $^{87}Sr/^{86}Sr$ plot, ranging from 0.5125 to 0.5130 and from 0.7036 to 0.7047, respectively (Figure 5c). In detail, volcanic products of the Western Cordillera and back-arc regions present the least radiogenic Sr and most radiogenic Nd compositions ($^{87}Sr/^{86}Sr$: 0.7038–0.7044 and $^{143}Nd/^{144}Nd$: 0.5128–0.51295), whereas Eastern cordillera volcanoes display slightly more radiogenic Sr ($^{87}Sr/^{86}Sr$: 0.7041–0.7047) and unradiogenic Nd values ($^{143}Nd/^{144}Nd$: 0.51255–0.51285). Within this isotope space, it is impossible to distinguish back-arc and Western Cordillera volcanoes but there is a clear division between Western Cordillera—back-arc and Eastern Cordillera volcanoes at $^{143}Nd/^{144}Nd = 0.5128$ (Figure 5c). In addition, Inter-Andean valley volcanoes plot within the field of the Western Cordillera—back-arc cluster apart from samples from Huisla volcano, which shows some affinity with the Eastern Cordillera. The isotopic compositions for Cotopaxi and Licto are transitional between the Western Cordillera—back-arc and the Eastern Cordillera clusters.

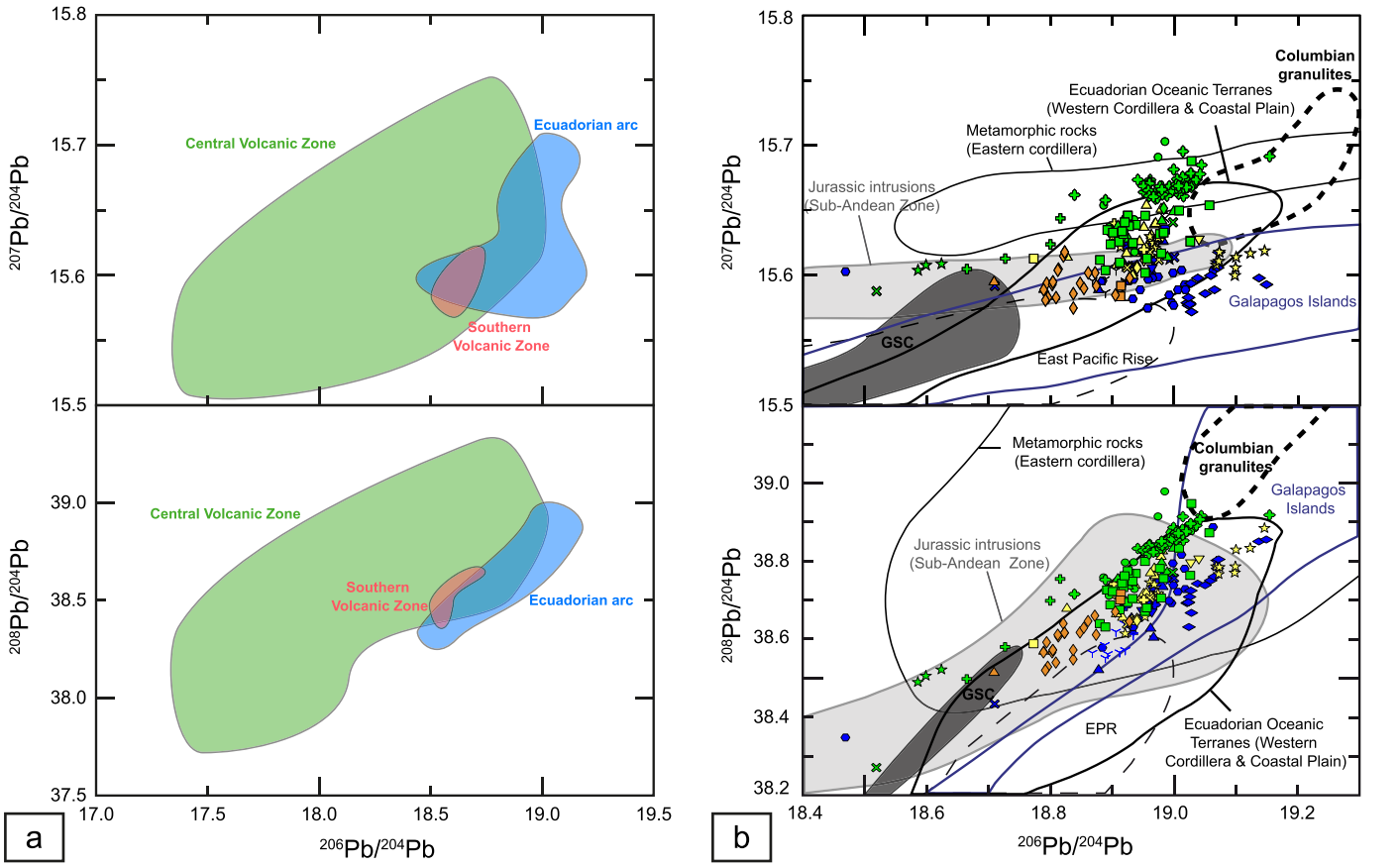

Figure 6. Pb isotopic compositions of Ecuadorian volcanic products. Data are from the literature (see references for Figure 3) and new data from this study (supporting information); compositional fields are taken from *Chiaradia et al.* [2009] in Figure 6b and from literature data (see references Figure 3) in Figure 6a. Legend as in Figure 3.

The Sr-Nd isotopic compositions of the Ecuadorian volcanic products are also compared to those of the crustal rocks of the Northern Andes as well as the adjacent oceanic domains (Figure 5b). All Ecuadorian samples plot at the edge of the Columbian lower crustal xenolith field [*Weber et al.*, 2002]. Western Cordillera basement rocks [*Chiaradia et al.*, 2004] cover a very wide range of $^{87}Sr/^{86}Sr$ values (0.703–0.706) and have radiogenic Nd values (mostly $^{143}Nd/^{144}Nd > 0.5129$). The volcanic products with the most radiogenic Nd of the Western Cordillera plot within this latter field. Pilavo and Puñalica lavas, which have the least radiogenic Sr values, have compositions close to the Galapagos Islands field [*White et al.*, 1993] and to Western Cordillera basement rocks [*Reynaud et al.*, 1999; *Chiaradia et al.*, 2004].

4.3. Pb Isotopes

Ecuadorian volcanoes are much more homogeneous in lead isotopic composition than the Central Volcanic Zone volcanoes but more diverse than the Southern Volcanic Zone ones (Figure 6a). Ecuadorian samples display the most radiogenic $^{206}Pb/^{204}Pb$ values amongst the Andean chain products while they have intermediate $^{207}Pb/^{204}Pb$ and $^{208}Pb/^{204}Pb$ compositions. Figure 6b shows lead isotopic data from Ecuador, including both literature and new data. Almost all Western Cordillera and back-arc volcanoes display very homogeneous $^{207}Pb/^{204}Pb$ (15.58–15.63) while $^{206}Pb/^{204}Pb$ compositions vary significantly (from 18.47 to 19.15). In contrast, most Inter-Andean Valley and Eastern Cordillera volcanic centers display a large range of $^{207}Pb/^{204}Pb$ values (from 15.59 to 15.70) with little $^{206}Pb/^{204}Pb$ variation (18.95–19.05). In the $^{207}Pb/^{204}Pb$ versus $^{206}Pb/^{204}Pb$ space (Figure 6b), these two trends intersect at $^{206}Pb/^{204}Pb = 18.85–18.97$ and $^{207}Pb/^{204}Pb = 15.585–15.625$. Interestingly, these Pb isotopic signatures correspond to back-arc isotopic compositions, represented by Sumaco and Conos de Puyo volcanoes. The highest $^{207}Pb/^{204}Pb$ values are found at Tungurahua and Antisana whereas the most radiogenic ^{206}Pb samples are from Pilavo and Imbabura in the northern part of the Western Cordillera.

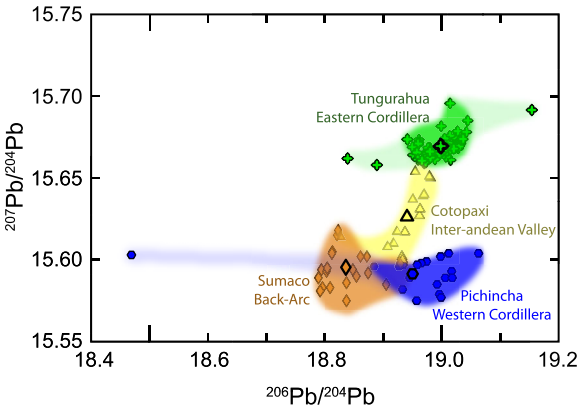

Figure 7. Intravolcano isotopic variability for Pichincha, Sumaco, Cotopaxi, and Tungurahua volcanoes in $^{207}Pb/^{204}Pb$ versus $^{206}Pb/^{204}Pb$ space. All compositions are displayed as well as mean values for each volcano. Legend as in Figure 3.

In general, back-arc volcanoes along with Reventador, on the margin of the Eastern Cordillera, seem to display the least radiogenic $^{206}Pb/^{204}Pb$ compositions, whereas Western Cordillera volcanic centers define the other end of this trend. Thus, our new lead isotopic data allow us to distinguish Western Cordillera volcanic centers from Eastern Cordillera ones, as well as those from the back-arc (Figure 6). The same trends are observed within the $^{208}Pb/^{204}Pb$ versus $^{206}Pb/^{204}Pb$ space.

Eastern Cordillera metamorphic rocks have radiogenic $^{207}Pb/^{204}Pb$ values and show a wide range of $^{206}Pb/^{204}Pb$ compositions, matching Tungurahua and Antisana signatures (Figure 6b). Colombian granulites [*Weber et al.*, 2002] also have radiogenic $^{207}Pb/^{204}Pb$ values (15.62–15.75) and slightly higher $^{206}Pb/^{204}Pb$ than Eastern Cordillera and Inter-Andean valley volcanic products (19.0–19.3). Western Cordillera basement covers the majority of the range in Ecuadorian lead isotopic compositions except for the extremities of the three trends described above. Only some Galapagos Islands rocks are enriched in ^{206}Pb without being enriched in ^{207}Pb; Pilavo, Imbabura, and Pichincha rocks plot within this field. Finally, Reventador, Sangay, and Soche have higher $^{207}Pb/^{204}Pb$ than the Galapagos Spreading Center and the East Pacific Rise but are similar to Jurassic intrusions in the sub-Andean zone.

5. Geographical Distribution of Sr-Nd-Pb Signatures in Ecuador

5.1. Preliminary Data Treatment

Here we propose a geographical approach aimed at comparing isotopic variations across the arc (E-W) with those along the arc (N-S). In order to show Sr-Nd-Pb isotopic variations on a map, we take the average value for each volcanic center.

Individual volcanoes display a restricted range of isotopic variations and can be distinguished from each other (Figures 5–7). We focus first on lead compositions, which best discriminate Western Cordillera, Eastern Cordillera, and back-arc eruptive products. To illustrate our approach, we selected one volcano from each alignment: Pichincha (Western Cordillera), Cotopaxi (at the boundary between the Inter-Andean valley and the Eastern Cordillera), Tungurahua (Eastern Cordillera), and Sumaco (back arc). These volcanoes are well-documented for their lead isotopic compositions: 20 samples for Pichincha [this paper; *Chiaradia et al.*, 2009; *Bourdon et al.*, 2002a; *Bryant et al.*, 2006], 16 for Cotopaxi [*Garrison et al.*, 2011; *Bryant et al.*, 2006], 64 for Tungurahua (this paper; and Nauret, personal communication) and 23 for Sumaco [this paper; unpublished IRD data; *Chiaradia et al.*, 2009; *Bryant et al.*, 2006; *Bourdon et al.*, 2003]. For each volcano, we show mean isotopic composition and individual data points in Figure 7, allowing a comparison of intravolcano and intervolcano isotopic variability. This highlights the fact that the intravolcano isotopic variability is smaller than the intervolcano variability and that the difference between each volcanic center is accurately represented by the average values.

Table 1 summarizes the average Pb isotopic composition for each edifice. In some cases, data for individual volcanoes are not regularly distributed around the mean. For example, Imbabura samples plot in two distinct clusters, which may reflect two distinct populations [cf. *Bryant et al.*, 2006]. In addition, when only two samples are analyzed for lead isotopic compositions and the results are very different, the significance of an average is debatable. Fortunately this rarely occurs in our data set (only observed for Cotocachi and Soche volcanoes) (Figure 6 and Table 1).

Most importantly, we emphasize that intravolcano variability does not overlap the large variability of lead isotopic compositions observed throughout the arc and that the spatial distribution of average

Table 1. Average Values of Volcano Isotopic Compositions[a]

Volcano		$^{87}Sr/^{86}Sr$	$^{143}Nd/^{144}Nd$	$^{206}Pb/^{204}Pb$	$^{207}Pb/^{204}Pb$	$^{208}Pb/^{204}Pb$	$\delta^{18}O$	Majors-Traces No. Samples Max
Almas Santas	No. samples	6	5	1	1	1	5	27
	Mean	0.70404	0.51288	18.96	15.625	38.72	7.32	
	1 SD	0.00016	0.00004				0.93	
Atacazo	No. samples	30	30	5	5	5	23	128
	Mean	0.70424	0.51286	18.94	15.604	38.62	8.29	
	1 SD	0.00007	0.00002	0.04	0.014	0.08	0.72	
Carihuairazo	No. samples	1	1	1	1	1	0	31
	Mean	0.70410	0.51284	18.99	15.635	38.77		
Casitagua	No. samples	1	1	1	1	1	0	1
	Mean	0.70414	0.51291	18.93	15.606	38.65		
Chachimbiro	No. samples	4	4	4	4	4	0	11
	Mean	0.70399	0.51293	19.03	15.611	38.77		
	1 SD	0.00005	0.00001	0.04	0.001	0.03		
Chiles/Cerro Negro	No. samples	0	0	0	0	0	0	21
Chimborazo	No. samples	0	0	0	0	0	5	145
	Mean						7.76	
	1 SD						0.25	
Corazon/Cerro Bombo	No. samples	1	1	1	1	1	0	5
	Mean	0.70412	0.51288	18.92	15.622	38.68		
Cotacachi	No. samples	2	1	2	2	2	0	10
	Mean	0.70398	0.51291	18.86	15.603	38.60		
	1 SD	0.00019		0.21	0.016	0.23		
Cuicocha	No. samples	2	2	2	2	2	0	20
	Mean	0.70430	0.51291	18.97	15.612	38.69		
	1 SD	0.00002	0.00001	0.00	0.001	0.00		
Iliniza	No. samples	7	7	3	3	3	13	60
	Mean	0.70412	0.51287	18.96	15.613	38.68	8.40	
	1 SD	0.00010	0.00001	0.01	0.006	0.01	0.61	
Pichincha	No. samples	35	35	20	20	20	10	165
	Mean	0.70403	0.51289	18.95	15.591	38.69	7.59	
	1 SD	0.00005	0.00002	0.12	0.010	0.11	0.23	
Pilavo	No. samples	15	15	15	15	15	0	40
	Mean	0.70387	0.51293	19.05	15.590	38.74		
	1 SD	0.00004	0.00001	0.04	0.013	0.06		
Pululahua	No. samples	11	11	11	11	11	0	11
	Mean	0.70414	0.51291	18.91	15.599	38.59		
	1 SD	0.00003	0.00002	0.02	0.008	0.03		
Quilotoa	No. samples	2	2	2	2	2	0	14
	Mean	0.70402	0.51287	18.98	15.634	38.73		
	1 SD	0.00001	0.00002	0.01	0.015	0.03		
Calpi	No. samples	1	1	1	1	1	0	20
	Mean	0.70408	0.51283	18.90	15.637	38.73		
Cotopaxi	No. samples	9	10	16	16	16	0	16
	Mean	0.70422	0.51280	18.94	15.626	38.73		
	1 SD	0.00013	0.00010	0.04	0.018	0.06		
Huisla	No. samples	1	1	1	1	1	0	56
	Mean	0.70416	0.51274	18.77	15.613	38.59		
Ilalo	No. samples	5	5	4	4	4	0	5
	Mean	0.70408	0.51286	18.95	15.612	38.68		
	1 SD	0.00004	0.00005	0.01	0.007	0.03		
Imbabura	No. samples	16	16	16	16	16	0	16
	Mean	0.70410	0.51289	19.02	15.617	38.75		
	1 SD	0.00007	0.00003	0.08	0.009	0.07		
Licto	No. samples	1	1	1	1	1	0	7
	Mean	0.70415	0.51282	18.90	15.640	38.74		
Mojanda - Fuya Fuya	No. samples	9	9	3	3	3	4	92
	Mean	0.70416	0.51290	18.95	15.612	38.69	8.80	
	1 SD	0.00006	0.00002	0.03	0.006	0.04	0.35	
Pasochoa	No. samples	1	1	1	1	1	1	21
	Mean	0.70409	0.51289	18.95	15.620	38.70	7.5	
Puñalica	No. samples	3	3	3	3	3	3	38
	Mean	0.70382	0.51290	19.02	15.629	38.79	6.97	
	1 SD	0.00022	0.00002	0.03	0.001	0.02	0.12	
Antisana	No. samples	22	22	8	8	8	2	27
	Mean	0.70437	0.51275	18.93	15.654	38.81	6.40	
	1 SD	0.00011	0.00003	0.03	0.029	0.09	0.42	

Table 1. (continued)

Volcano		$^{87}Sr/^{86}Sr$	$^{143}Nd/^{144}Nd$	$^{206}Pb/^{204}Pb$	$^{207}Pb/^{204}Pb$	$^{208}Pb/^{204}Pb$	$\delta^{18}O$	Majors-Traces No. Samples Max
Cayambe	No. samples	17	17	5	5	5	6	175
	Mean	0.70438	0.51274	18.96	15.634	38.78	7.18	
	1 SD	0.00010	0.00005	0.04	0.014	0.04	0.38	
Chacana	No. samples	26	27	27	27	27	0	27
	Mean	0.70432	0.51275	18.94	15.632	38.74		
	1 SD	0.00016	0.00005	0.05	0.018	0.07		
Chalupas	No. samples	2	2	2	2	2	0	2
	Mean	0.70445	0.51275	18.99	15.660	38.85		
	1 SD	0.00003	0.00001	0.01	0.012	0.03		
Reventador	No. samples	3	3	3	3	3	0	18
	Mean	0.70452	0.51277	18.60	15.607	38.51		
	1 SD	0.00002	0.00002	0.02	0.003	0.02		
Sangay	No. samples	14	14	4	4	4	0	97
	Mean	0.70433	0.51273	18.75	15.622	38.63		
	1 SD	0.00009	0.00003	0.07	0.017	0.12		
Soche	No. samples	2	2	2	2	2	0	11
	Mean	0.70440	0.51278	18.76	15.615	38.52		
	1 SD	0.00002	0.00003	0.34	0.037	0.35		
Tungurahua	No. samples	22	22	64	64	64	13	64
	Mean	0.70427	0.51276	19.00	15.669	38.86	7.57	
	1 SD	0.00004	0.00002	0.04	0.007	0.03	0.29	
Pan de Azucar	No. samples	2	2	2	2	2	0	25
	Mean	0.70410	0.51289	18.75	15.592	38.54		
	1 SD	0.00005	0.00004	0.06	0.004	0.04		
Puyo	No. samples	2	2	2	2	2	0	33
	Mean	0.70385	0.51287	18.91	15.588	38.71		
	1 SD	0.00002	0.00000	0.00	0.006	0.01		
Sumaco	No. samples	33	33	23	23	23	2	38
	Mean	0.70416	0.51289	18.84	15.595	38.60	6.20	
	1 SD	0.00006	0.00001	0.04	0.011	0.04	0.00	
Azufral de Tuquerres	No. samples	0	0	0	0	0	0	10
Cumbal	No. samples	0	0	0	0	0	0	5
Doña Juana	No. samples	0	0	0	0	0	0	4
Galeras	No. samples	0	0	0	0	0	0	25

[a]For each volcano, number of samples and standard deviation of isotopic data are given. Number of samples used for calculation of average major and trace element composition is also shown. The significance of each mean depends on the number of samples used. We choose to include all existing data even though some seem to be outliers (cf. Figure 7, Pichincha data). Obviously, statistical means can be used to decide whether or not to include a sample, based on a Gaussian distribution for data. However, there is no objective reason that such an assumption is valid for natural data. Data filtering would also require an equivalent level of knowledge of each volcano, sampling and analytical methods, which is (1) beyond the level of detail aimed at in this study, and (2) difficult to achieve here as most of data are taken from the literature.

compositions is meaningful (cf. standard deviations in Table 1). Thus, maps representing the isotopic diversity of Ecuador are drawn up by using the average isotopic composition for each volcano. Isotopic composition ranges are color-coded, choosing a variation range equal to or higher than the mean standard deviation within volcanoes. Hence, differences between colors are mathematically significant and we traced isovalues lines so as to define color (i.e., compositional) limits.

5.2. Across-Arc Versus Along-Arc Variations

Previous studies have shown that the two Cordilleras can be distinguished based on Sr, Nd, and O isotopes [cf. *Bourdon et al*., 2003; *Hidalgo et al*., 2012]. Nevertheless, the signatures of the Western Cordillera and back-arc volcanoes overlap to a large extent. Across-arc studies [*Bourdon et al*., 2003; *Bryant et al*., 2006; *Chiaradia et al*., 2009; *Hidalgo et al*., 2012] have focused on Sumaco as the reference back-arc volcano. However, these studies did not take into account the geochemical and isotopic variations that occur along the arc, namely the differences between the Pan de Azucar, Sumaco, and Conos de Puyo volcanoes in the back-arc or the large difference in Western Cordillera volcanoes (e.g., Pilavo and Carihuairazo) (Figures 5 and 6).

Figure 8 displays geographical variations of $^{87}Sr/^{86}Sr$ and $^{143}Nd/^{144}Nd$. The $^{143}Nd/^{144}Nd$ ratio is the lowest along a N-S axis formed by the Cayambe, Chalupas, Huisla, and Sangay volcanoes, and increases on both sides of this line. The most radiogenic Sr isotopic compositions (up to $^{87}Sr/^{86}Sr = 0.70466$ in Chacana volcano) are found in the Eastern Cordillera while unradiogenic values occur in the Western Cordillera and in the

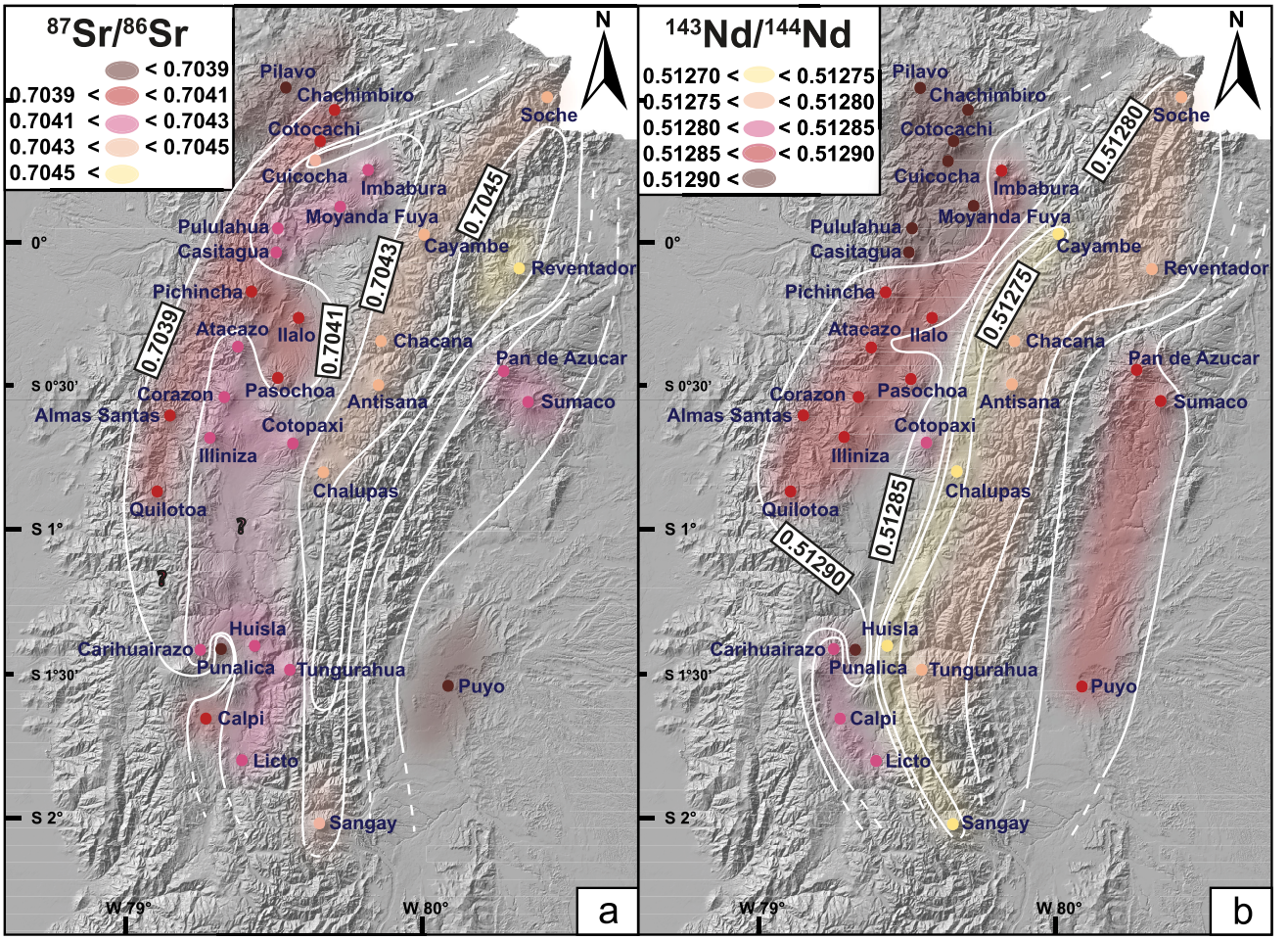

Figure 8. Schematic map showing the distribution of (a) $^{87}Sr/^{86}Sr$ and (b) $^{143}Nd/^{144}Nd$ compositions in Ecuador.

Conos de Puyo in the back arc. All isotope maps clearly confirm that the main Sr-Nd isotopic variability is along the E-W axis.

We also note a general southward decrease in $^{87}Sr/^{86}Sr$ along the Eastern Cordillera and especially along the back-arc region. Meanwhile $^{143}Nd/^{144}Nd$ generally decreases toward the south along the Western Cordillera, from Pilavo to Carihuairazo. In contrast, Nd isotopic data for the Eastern Cordillera display rather homogeneous values from north to south.

Instead of showing raw Pb data, Figure 9b shows the distribution of four major Pb signatures distinguished in $^{207}Pb/^{204}Pb$ versus $^{206}Pb/^{204}Pb$ diagram (Figure 9a). We define these fields to analyze sample distribution along the two Pb-Pb trends described above (Figure 9c). The map highlights the already recognized differences between the Western Cordillera, the Eastern Cordillera and the back arc, but also highlights the latitudinal changes.

The frontal part of the arc (Western Cordillera and most of the Inter-Andean valley edifices) is divided into two main sectors: the northern part displays radiogenic $^{206}Pb/^{204}Pb$ and unradiogenic $^{207}Pb/^{204}Pb$ (blue and violet sectors in Figure 9c) while the southern part displays radiogenic $^{206}Pb/^{204}Pb$ and radiogenic $^{207}Pb/^{204}Pb$ signatures (green sector in Figure 9c). The northernmost volcanoes of the frontal part of the arc display the highest $^{206}Pb/^{204}Pb$ (violet sector in Figure 9c). These variations resemble those observed for the Nd isotopes. The Eastern Cordillera is quite homogeneous, displaying radiogenic $^{207}Pb/^{204}Pb$

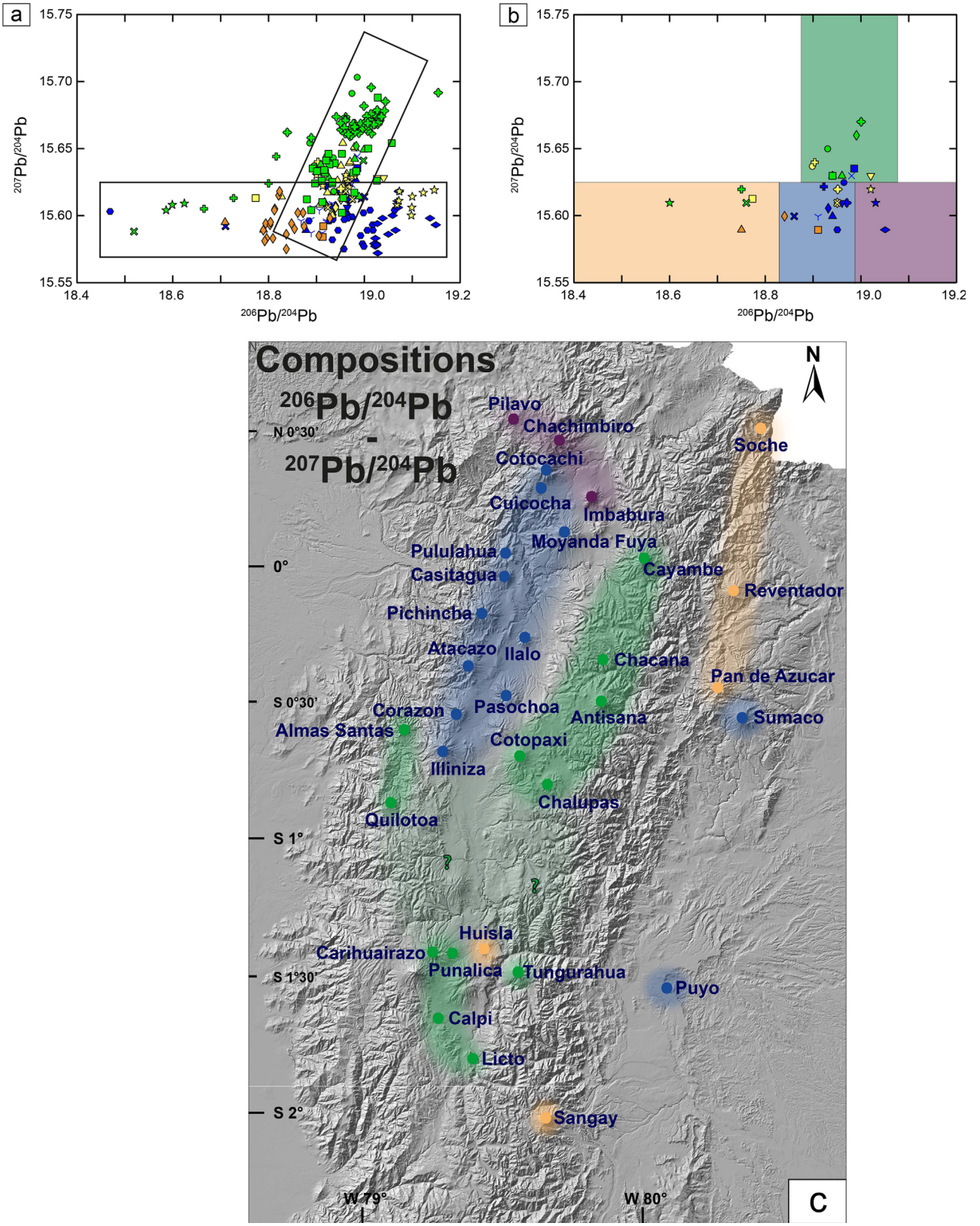

Figure 9. (a) $^{207}Pb/^{204}Pb$ versus $^{206}Pb/^{204}Pb$ diagram displaying Ecuadorian volcanic products (detail of Figure 6) and highlighting the trends discussed in the text. (b) $^{207}Pb/^{204}Pb$ versus $^{206}Pb/^{204}Pb$ diagram showing mean values for each volcano. Main isotopic signatures are color coded with blue representing the intersection of the two trends, and the other colors representing the extremities. (c) Geographical distribution of the main lead isotopic signatures; colors as in Figure 9b.

compositions. Volcanoes furthest from the trench, such as Sumaco and Conos de Puyo, have the same lead isotopic compositions as most of the northern volcanoes of the Western Cordillera. Volcanic centers located on the eastern part of the Eastern Cordillera (Sangay, Reventador, Pan de Azucar, Soche) have lower $^{206}Pb/^{204}Pb$ and $^{207}Pb/^{204}Pb$ than the main part of this cordillera. It should be noted that the data for Soche and Huisla volcanoes should be interpreted with caution as there is only one sample for Huisla, and the two samples for Soche are very different from each other.

Comparison between Figures 8 and 9 emphasizes that geographic variations in Sr, Nd, and Pb isotopes do not coincide exactly. This might reflect the well-known decoupling between Sr-Nd and Pb isotopes and, to a lesser extent, the fact that Sr and Nd are not strongly correlated (Figure 5). The threshold values used to draw contour lines might also contribute to some extent to this geographical decoupling.

Figures 8 and 9 clearly show that the geochemical evolution across the Ecuador arc is dependent on latitude. Radiogenic $^{207}Pb/^{204}Pb$ is not present in the northernmost part of Ecuador, whereas it occurs elsewhere in the arc. On the contrary, radiogenic $^{206}Pb/^{204}Pb$ is only found Northern volcanoes. In contrast, in the southern part of Ecuador (south of 1°S), there is no distinction between the Western and Eastern Cordillera in terms of lead isotopes. The back-arc volcanoes do not have the same signature from north to south. Thus, the geochemical variation of lavas throughout the Ecuadorian arc cannot be explained by a single process such as crustal contamination or binary mixing.

6. Discussion

6.1. The Crustal Imprint

Previous works [*Barragan et al*., 1998; *Bourdon et al*., 2003; *Bryant et al*., 2006; *Samaniego et al*., 2005; *Hidalgo et al*., 2012] have estimated the amount of upper crustal contamination in Ecuadorian magmas using different tools (trace elements and Sr-Nd-O isotopes). This amount is similar throughout Ecuador, ranging from 7 to 14 vol % in the Western Cordillera and from 6 to 13 vol % in the Eastern Cordillera according to *Hidalgo et al*. [2012]. Most of those studies agree that upper crustal assimilation plays a key role in magma evolution but does not overprint slab and mantle signatures.

Concerning lead isotopes, the most striking feature in Figure 9 is the similarity in lead isotopic composition ($^{206}Pb/^{204}Pb$: 18.95–19.00; $^{207}Pb/^{204}Pb \geq 15.63$; green field in Figure 9) between the southern volcanoes of the frontal part of the arc and the volcanoes of the Eastern Cordillera, despite their having contrasted basements in terms of lithology (oceanic and continental, respectively) and lead isotopic signature (roughly $^{207}Pb/^{204}Pb < 15.65$ and $^{207}Pb/^{204}Pb > 15.65$, respectively, cf. Figure 6). Thus, the geographical distribution of lead isotopic signatures suggests that upper crustal contamination is not the main parameter controlling the lead isotopic composition of Ecuadorian magmas. Since this trend lies in the direction of the Columbian granulites field (Figure 6), which are interpreted as having a lower crustal origin [*Weber et al*., 2002], we propose that magmas acquire their signature (high $^{207}Pb/^{204}Pb$ values) at lower crustal levels by a process such as that proposed by *Hildreth and Moorbath* [1988] and more recently by *Annen et al*. [2006]. This model includes processes of accumulation, recycling, fractionation, and assimilation of crustal material in the so-called deep crustal hot zones. In addition, acquirement of higher $^{207}Pb/^{204}Pb$ at mantle level is unlikely because mantle components have low $^{207}Pb/^{204}Pb$ [*Hofmann*, 1997]. Hence, volcanoes located in the Eastern Cordillera and the south of the frontal part of the arc would inherit their isotopic signature from the lower crust, which is in agreement with their more radiogenic Sr and unradiogenic Nd compositions (Figure 8).

The group that is characterized by unradiogenic $^{206}Pb/^{204}Pb$ and $^{207}Pb/^{204}Pb$ compositions (Pan de Azucar, Reventador, Huisla, Sangay, and Soche; orange field in Figure 9) could also have inherited their signature from the upper crust. Indeed, in Figure 6, the only geological unit corresponding to this composition is represented by the Jurassic intrusions of the sub-Andean zone [*Chiaradia et al*., 2004], whose radiogenic Sr compositions also support this idea (Figure 5).

In conclusion, radiogenic $^{207}Pb/^{204}Pb$ compositions in Ecuadorian samples reflect the imprint of lower crustal assimilation, which seems significant in the south of the frontal part of the arc and in the main arc, while unradiogenic $^{206}Pb/^{204}Pb$ and $^{207}Pb/^{204}Pb$ compositions would reflect upper crustal contamination in the eastern Ecuadorian arc.

Table 2. Comparison of Across-Arc and Along-Arc Isotopic Variability for the Whole Arc[a]

	$^{87}Sr/^{86}Sr$	$^{143}Nd/^{144}Nd$	$^{206}Pb/^{204}Pb$	$^{207}Pb/^{204}Pb$	$^{208}Pb/^{204}Pb$
Across-Arc Variation (0.2°S) (%)	73	94	87	98	89
Along-arc Volcanic Front (%)	71	33	99	55	76
Along-arc Main Arc variation (%)	63	78	93	88	100
Along-arc Back Arc variation (%)	57	14	32	33	29

[a]We calculated variations taking all samples from the volcanic edifices chosen for each transect (one across-arc transect and three along-arc transects). The across-arc variability was calculated taking volcanic products from edifices located along a transect at about 0.2°S (namely Atacazo, Pichincha, Pasochoa, Ilalo, Antisana, Chacana, Pan de Azucar, Sumaco), which was used in previous publications for assessing the across-arc geochemical variations. We calculated along-arc variations for the frontal part of the arc, the main arc and the back arc. Then, the difference between minimum and maximum for each transect was normalized to the whole arc variation (maximum-minimum).

6.2. Variation of the Slab Input into the Mantle Wedge

After having discriminated the isotopic compositions inherited from the arc crust, we now focus on deeper processes in the mantle wedge and the subducting slab. Quantitatively, we compare across-arc and along-arc isotope variability to variations in the arc as a whole (normalized to 100%) in Table 2 (details of the calculation in the caption of Table 2). Variability in $^{87}Sr/^{86}Sr$, $^{207}Pb/^{204}Pb$, and $^{143}Nd/^{144}Nd$ are greater across-arc (73%, 98% and 94%, respectively) than along-arc (57–71%, 33–88%, and 14–78%, respectively). However, along-arc variations in the frontal part of the arc encompass 99% of $^{206}Pb/^{204}Pb$ variability in the whole arc compared to 88% across the arc.

6.2.1. Across-Arc Variations

Trace elements show two across-arc trends that have been extensively discussed. First, the general increase of incompatible elements (LILE, HFSE; e.g., Ba, Th, Rb, Pb, Nb) toward the back-arc region (Figure 4) has been interpreted as being due to a decrease in slab input into the mantle wedge resulting in lower degrees of partial melting [*Barragan et al*., 1998; *Bourdon et al*., 2003; *Bryant et al*., 2006; *Le Voyer et al*., 2008; *Chiaradia et al*., 2009; *Hidalgo et al*., 2012]. This is a common feature in arcs worldwide [*Dickinson*, 1975; *Stolper and Newman*, 1994; *Davidson and De Silva*, 1995; *Ryan et al*., 1995]. The low degree of melting of the back-arc mantle would explain the extreme enrichment in incompatible elements in the back-arc volcanics.

Second, the enrichment of aqueous fluid-mobile over aqueous fluid-immobile elements (Ba/Th, Figure 4; Ba/Nb, Ba/La, Pb/Th, Pb/La, Cs/Th, Cs/Nb, Li/Th, not shown) in the frontal part of the Ecuadorian arc suggests an early release of fluid-mobile elements from the slab and extensive slab dehydration below the frontal part of the arc. However, it does not rule out the possibility of a simultaneous input of silicate melt from the slab into the mantle wedge. Indeed, as the slab sinks into the mantle, some portions of the oceanic crust might undergo dehydration while others might melt [*Elliot et al*., 1997; *Kelemen et al*., 2014; *Spandler and Pirard*, 2013]. As a result, the invoked "slab-component" released into the mantle wedge could be highly variable in composition. In fact, it may be either an aqueous-dominated fluid or a hydrous silicate melt, depending on the thermal regime of the subducting slab. Trace element partitioning during slab processing depends on their mobility in aqueous fluids or their affinity for silicate melts [*Kessel et al*., 2005]. The highly contrasting behavior of elements during slab descent yields a marked and systematic chemical evolution of the slab-component across the arc [*Kessel et al*., 2005; *Kelley et al*., 2005]. Consequently, ratios such as Ba/Th indicate an input of aqueous fluid into the mantle wedge since Ba is mobile in any kind of fluid or melt while Th is only mobile in silicate melts [cf. *Kessel et al*., 2005]. Volcanoes in the frontal part of the arc display higher Ba/Th ratios than those further from the trench (Figure 4), thus the subducted slab is dehydrating extensively beneath the frontal part of the arc. Yet, high ratios of Ba/Th are also observed at the Conos de Puyo volcano in the back arc, but these values reflect a constantly low Th content ($Th < 8$ ppm) compared to other incompatible elements which are enriched and highly variable (for instance, Ba: 580–2774 ppm) rather than an extensively dehydrating slab beneath the back-arc region. In fact, the magma source of Conos de Puyo is believed to be a hydrated phlogopite-bearing and garnet-bearing lherzolite, which accounts for the extreme enrichment in Ba and other incompatible elements [*Hoffer et al*., 2008].

Element partitioning between slab and fluids might also influence the isotopic budget of the fluids expelled from the slab. Pb and Sr are more mobile than Nd (in both types of fluids) [*Kessel et al*., 2005]. Normally, Pb and to a lesser extent Sr, are released early in the front arc mantle, whereas Nd is released further from the trench [*Kelley et al*., 2005]. Hence, at constant volume of fluids released by the slab, the influence of the slab

component on Pb and Sr isotopic compositions would be greater in the frontal arc than in the back arc. Thus, the isotopic systems record slab fluid input across the arc with variable sensitivity, depending on the balance of Sr, Nd, or Pb inherited from the slab, the mantle and the crust. In the Ecuadorian arc, the across-arc isotopic variability, at least in Sr and Nd, is mainly controlled by crustal influence [*Bryant et al*., 2006; *Chiaradia et al*., 2009; *Hidalgo et al*., 2012]. The highest $^{87}Sr/^{86}Sr$ and $^{207}Pb/^{204}Pb$, and lowest $^{143}Nd/^{144}Nd$ are indeed found in the Eastern Cordillera (Figures 8 and 9), where magmas seem to be most highly contaminated (upper and lower crust). Conversely, across-arc variations in $^{206}Pb/^{204}Pb$ seem mainly to record mantle wedge compositions rather than crustal processes.

6.2.2. Along-Arc Variations

A more detailed study of the evolution of slab input along the Ecuadorian arc is possible in the frontal arc volcanoes since along-arc geochemical variations further to the trench seem related to crustal contamination. Based on Sr-Nd-Pb isotopic data, crustal contamination in the northern part of the frontal part of the arc is low and does not overprint the isotopic signatures of the mantle-derived melts. Hence, isotopic compositions in that region must be inherited from the mantle wedge variably metasomatized by slab aqueous fluids or silicate melts. The composition of the mantle beneath the Ecuadorian arc is expected to correspond to the blue-violet field in Figure 9b ($^{206}Pb/^{204}Pb = 18.8–19.2$; $^{207}Pb/^{204}Pb = 15.575–15.625$). As pointed out above, more than 50% of the Pb in the slab is released beneath the frontal part of the arc [*Kelley et al*., 2005], making Pb isotopic composition of the mantle wedge very sensitive to addition of slab aqueous fluids or melts.

Pilavo, Imbabura, and Chachimbiro volcanoes, all located in the northern part of the frontal arc, plot at the high $^{206}Pb/^{204}Pb$ end of the mantle field (Figure 9a). This signature cannot be explained by crustal contamination from the oceanic basement whose $^{206}Pb/^{204}Pb$ does not exceed 19.1 (Macuchi terrane, *Chiaradia* [2009]). Samples from the Galapagos Islands (Figure 6b) [*White et al*., 1993; *Werner et al*., 2003] are the only ones displaying this type of signature (high $^{206}Pb/^{204}Pb$, relatively low $^{207}Pb/^{204}Pb$). It is thus possible that the mantle beneath the northernmost part of Ecuador is influenced by the Carnegie Ridge oceanic crust. In Costa Rica, *Gazel et al*. [2015] suggested a similar feature. The onset of the Cocos Ridge's subduction strongly modified magma geochemistry, shifting erupted products from basalts with local MORB lead isotopic compositions to andesites displaying higher $^{206}Pb/^{204}Pb$ and fractionated La/Yb. If the Carnegie ridge impacts the isotope composition of the mantle wedge, we do not exclude an influence of slab sediments, whose isotopic composition is unknown. However, they would affect in a small the slab component as the recent work of *Proust et al*. [2016] showed that the sediment cap in front of the Ecuadorian margin is very thin ($\approx$100 m).

In frontal volcanoes samples, incompatible element contents and some trace element ratios (e.g., La/Yb, Sm/Yb) progressively increase away from 0.5°S latitude while fluid-mobile to fluid-immobile ratios decrease (Figure 4c). These trends are comparable to the increase in $^{206}Pb/^{204}Pb$ ratios away from $\sim$0°S–0.5°S, and contrast with the continuous increase in $^{207}Pb/^{204}Pb$ and decrease in $^{143}Nd/^{144}Nd$ from north to south (Figure 10). Thus, if the northward increase in $^{206}Pb/^{204}Pb$ is related to a slab input, as postulated above, the southward increase in $^{206}Pb/^{204}Pb$ must derive from another process as it is associated with an increase in $^{207}Pb/^{204}Pb$ and a decrease in $^{143}Nd/^{144}Nd$. As proposed above, magmas appear to be contaminated by lower crust in the southern part of the frontal region, which is in agreement with the strongly coupled variations in $^{207}Pb/^{204}Pb$ and $^{143}Nd/^{144}Nd$. This could explain both isotopic compositions (more radiogenic $^{206}Pb/^{204}Pb$, $^{207}Pb/^{204}Pb$, $^{87}Sr/^{86}Sr$, and unradiogenic $^{143}Nd/^{144}Nd$ in the south) and the increase in incompatible trace elements (which are concentrated in the crust) toward the south. The increase in Sm/Yb in the southern part could also indicate the presence of garnet in the lower crust.

On the other hand, the northward trend (higher $^{206}Pb/^{204}Pb$ at constant $^{207}Pb/^{204}Pb$) could be linked to the nature and extent of slab input into the mantle wedge. Fluid-mobile to fluid-immobile ratios suggest that dehydration of the slab is maximum at around 0.5°S in the frontal part of the arc and decreases away from this latitude. As $^{206}Pb/^{204}Pb$ is negatively correlated with Ba/Th (Figure 11, and other fluid-mobile to fluid-immobile ratios, not shown), radiogenic $^{206}Pb/^{204}Pb$ could be carried by a siliceous melt originating from the basaltic crust of the slab. Galapagos island basalts are the only known source in the study area which carries this isotopic signature (radiogenic $^{206}Pb/^{204}Pb$ with $^{207}Pb/^{204}Pb < 15.65$). Metasomatism by a siliceous melt could also account for the progressive fractionation of Sm relative to Yb, which indicates partial melting in the garnet stability field, as well as the increase in incompatible element content toward the

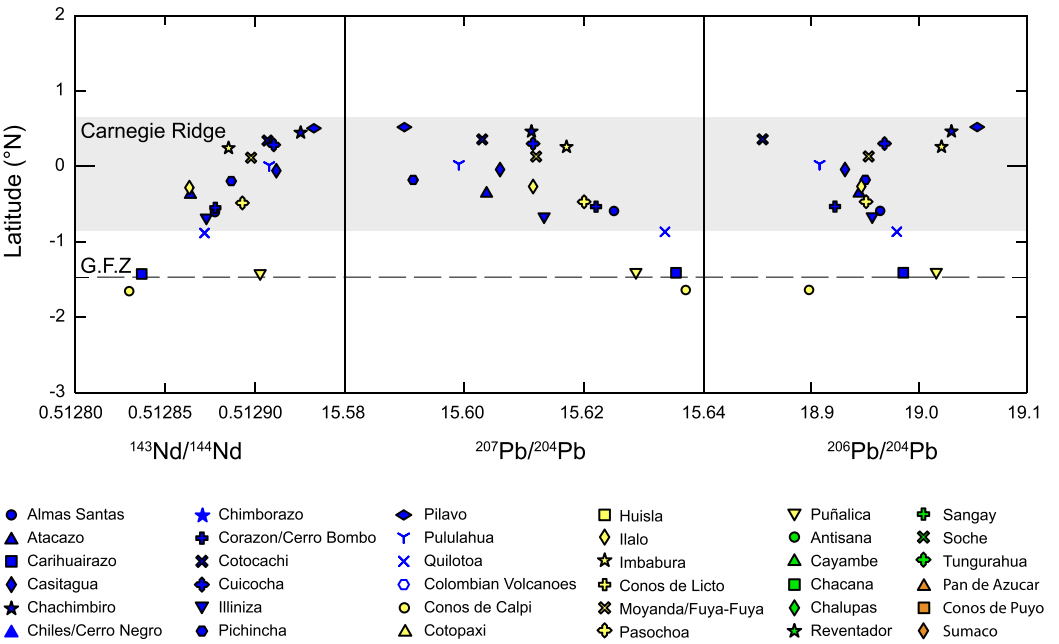

Figure 10. Mean compositions of $^{143}Nd/^{144}Nd$, $^{207}Pb/^{204}Pb$, and $^{206}Pb/^{204}Pb$ for volcanoes from the frontal part of the Ecuadorian arc displayed by latitude. Legend of Figure 3 displayed again.

north (fluid-mobile as well as fluid-immobile). Thus, the "slab component" would gradually evolve along the arc from a dominantly aqueous fluid in the middle of the frontal part of the arc (0.5°S) toward a dominantly siliceous melt to the north and to the south. The nature of the slab component in the southern termination of the frontal arc is more difficult to determine as magmas undergo modifications in the lower crust, which would overprint the slab signature. However, Ba/Th ratios indicate that extensive metasomatism of the mantle wedge by an aqueous fluid is unlikely in the south of the frontal arc.

Figure 12 summarizes source influences on isotopic compositions. Several trends are clearly distinguishable in the diagram. First, the decrease in $^{143}Nd/^{144}Nd$ at constant $^{206}Pb/^{204}Pb$ marks the lower crustal imprint upon the mantle signature. Second, mantle-derived magmas (bearing the lower crustal imprint or not) undergoing upper crustal contamination show a decrease in $^{206}Pb/^{204}Pb$ at constant $^{143}Nd/^{144}Nd$ (such as for some back-arc samples and samples erupted at the eastern edge of the Western Cordillera). Lastly, slab input increases both $^{206}Pb/^{204}Pb$ and $^{143}Nd/^{144}Nd$ in the mantle wedge.

6.3. The Role of the Subducted Slab on Ecuadorian Magmatism

The influence of the subducted slab structure on magmatism in Ecuador has been discussed since the pioneering works of *Hall and Wood* [1985] and *Barberi et al.* [1988]. However, these works lack of in-depth studies of the subducted slab geometry. The role of the Carnegie Ridge has been invoked to explain some characteristics of the Ecuadorian arc (for a critical review, see, *Michaud et al.* [2009]), such as the enhanced crustal deformation and uplift in the forearc region [*Pedoja et al.*, 2006], the Andean Cordillera [*Spikings et al.*, 2001] and the sub-Andean foothills [*Bès de Berc et al.*, 2005]; the northward sliding of the Northern Andean block along the Chingual-Cosanga-Pallatanga-Puná (CCPP) fault system [*Pennington*, 1981]; and the unusual geochemical signature of the Ecuadorian arc [*Gutscher et al.*, 1999; *Bourdon et al.*, 2003]. These last authors proposed that a flat slab subduction, induced by the presence of young and buoyant oceanic lithosphere, is responsible for a high geothermal gradient that favors slab partial melting and thus adakitic magmatism throughout the arc. Even though the flat slab model proposed by *Gutscher et al.* [1999] was revoked by *Guillier et al.* [2001], the origin of the adakitic signature is still controversial [*Bourdon et al.*, 2003; *Garrison and Davidson*, 2003; *Samaniego et al.*, 2005; *Bryant et al.*, 2006; *Chiaradia et al.*, 2009; *Samaniego et al.*, 2010; *Hidalgo et al.*, 2012].

In contrast, the influence of the Grijalva Fracture Zone (GFZ) on Ecuadorian magmatism has not been discussed in the literature. On the basis of new seismic data from a recently improved local seismic network,

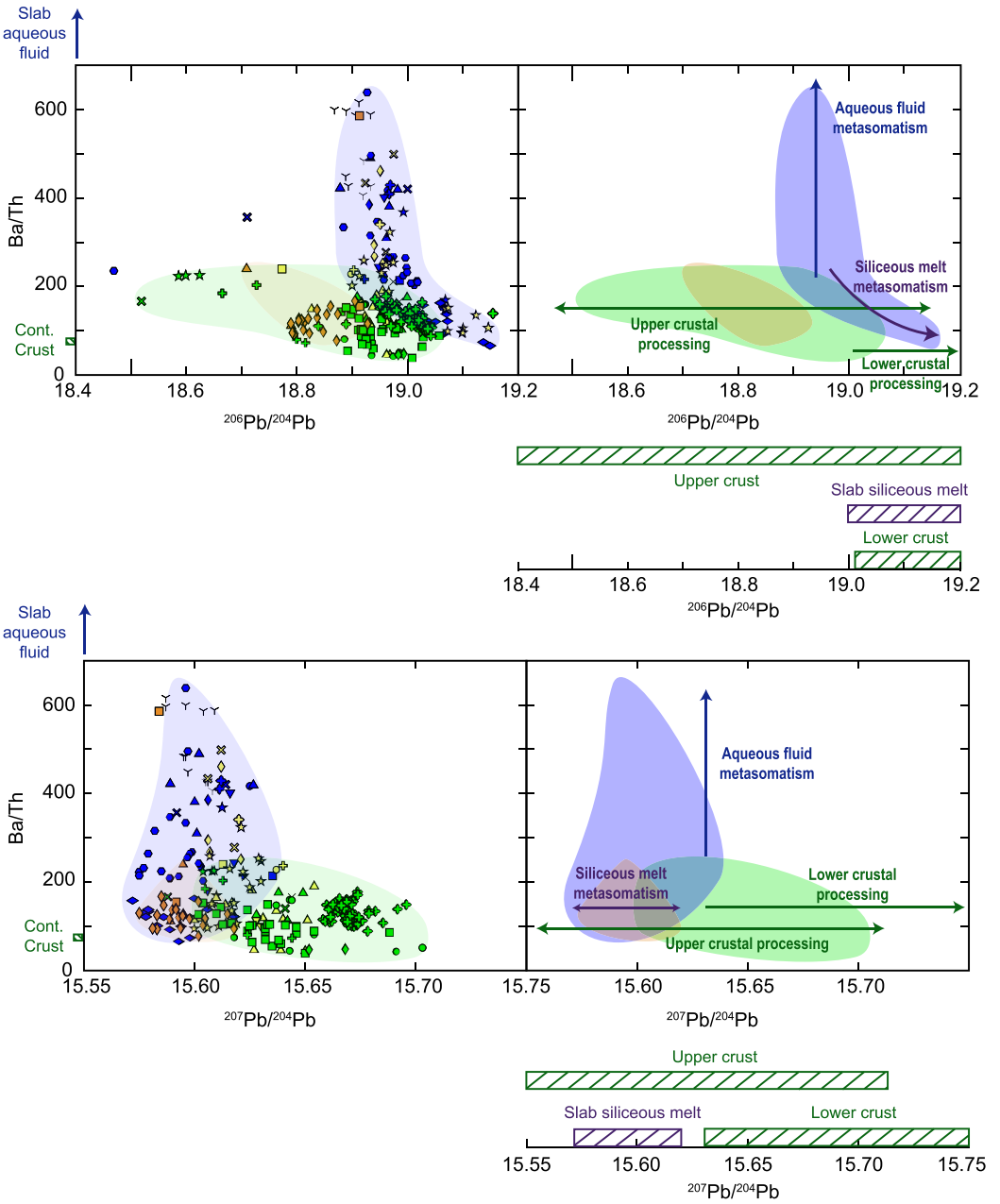

Figure 11. Ba/Th versus $^{206}Pb/^{204}Pb$ and $^{207}Pb/^{204}Pb$ of Ecuadorian samples, displaying the distinct influences of slab components (aqueous fluid or silicate melt) and arc crust on lead isotopic signatures of magmas. Ba/Th variation range in the continental crust was calculated after the determination of total crust estimates of *Taylor and McLennan* [1985], *Rudnick and Fountain* [1995], *Wedepohl* [1995], and *Rudnick and Gao* [2003]. Legend as in Figures 3 and 10.

Yepes et al. [2016] accurately define the geometry of the subducted slab beneath the active Ecuadorian arc. They show that the subducted slab displays flexure along the Grijalva Fracture Zone and that the inland projection of this structure lies beneath Puñalica and Chimborazo volcanoes in the Western Cordillera and extends between the Conos de Puyo and Sumaco volcanoes in the back-arc region. As a result, the depth of the slab is greatest along the GFZ and decreases away from it. The flexure of the slab would be due to differences in rheology between the oceanic crust on both sides of the GFZ and the change in convergence obliquity resulting from the convex shape of the continental margin. *Yepes et al.* [2016] stress that the older part of the Nazca plate, located south of 1°S, displays strong seismicity, while the subducted plate to the north of the Grijalva Fracture Zone is characterized by a lack of intermediate seismicity (80–150 km depth).

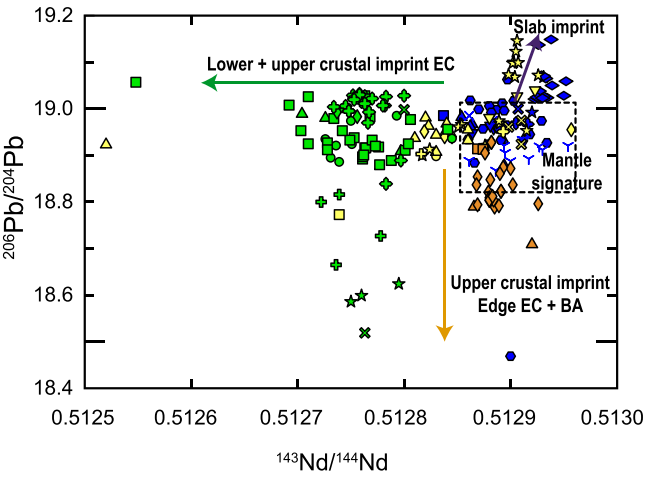

Figure 12. $^{143}Nd/^{144}Nd$ versus $^{206}Pb/^{204}Pb$ showing the different source influences on magma isotopic compositions in Ecuador. EC = Eastern Cordillera, BA = Back-Arc. Legend as in Figures 3 and 10.

The lack of seismicity along the Benioff plane is ascribed to the younger age of the Nazca plate, which is too hot and ductile to trigger large in-slab earthquakes [*Yepes et al*., 2016].

On the basis of this new geodynamic framework and the along-arc zonation described in this work, we propose that the older and probably colder Nazca plate (located south of the GFZ) may dehydrate and/or melt to a lesser extent than the younger Nazca plate (located north of the GFZ). As the Nazca plate decreases in age northwards, it is also possible that slab rheology changes progressively, with partial melting of the slab being favored as it becomes hotter northwards. Hence, production of siliceous melts in the slab would be enhanced in the northernmost part of the arc. This assumption is corroborated by the N-S variations described in the frontal part of the arc (N-S increase in incompatible element contents, greater fractionation of Sm over Yb and radiogenic $^{206}Pb/^{204}Pb$).

An additional observation is that the dip of the subducting slab determines the thickness of the mantle wedge beneath the active magmatic arc. The flux melting model proposed by *Grove et al*. [2002] suggests that fluids and/or melts from the subducted slab ascend by porous flow through the mantle wedge and continuously reequilibrate (thermally and chemically) with their surroundings. The final composition of the mantle-derived melts is thus influenced by the thermal state of the mantle wedge and by its width. This model was recently tested for the Chilean Southern Volcanic Zone by *Turner et al*. [2016] who conclude that the mantle-wedge thermal structure controls the trace-element budget in this arc segment. In Ecuador, the slab bends along the GFZ. Thus, this geometry may have an influence on the evolution of melts in the mantle wedge. The deeper the slab, the more extensive the melt-mantle equilibration, the more diluted the slab signature. This process could also explain why the slab isotopic signature is stronger in the northernmost volcanoes of the frontal arc. Conversely, mantle signatures are stronger in the back-arc region in Sumaco and Conos de Puyo, as well as in the middle of the frontal part of the arc (Figures 8 and 9), where the mantle wedge is thicker.

7. Quantitative Assessment of Source Contributions

7.1. Mass-Balance Model

We performed a principal component analysis (PCA) in five dimensions ($^{86}Sr/^{87}Sr$, $^{143}Nd/^{144}Nd$, $^{206}Pb/^{204}Pb$, $^{207}Pb/^{204}Pb$, $^{208}Pb/^{204}Pb$) to resolve the number of components needed to explain the dispersion of our data set. The PCA indicates that four components explain more than 99% of the variability. Thus, the contributions of upper crust, lower crust, mantle melts, and slab component at each volcanic center are evaluated in a mass-balance model. Mass-balance equations are solved in three-dimension ^{204}Pb-normalized isotope space using matrix formulation [*Vlastelic and Dosso*, 2005]. End-member choice is discussed hereafter and detailed in Table 3. We acknowledge that our model is very simple and does not take into account slab heterogeneity at local and regional scale, the progressive loss of Pb as the slab subducts [*Kelley et al*., 2005], and the small-scale compositional variations of the crustal basement. However, we prefer not to make poorly constrained assumptions that could distort the major, most important trends.

We choose the presumed depleted mantle isotopic composition beneath Galapagos Islands defined as DUM by *Harpp and White* [2001] as the reference mantle beneath Ecuador and use the average DMM Pb concentration calculated by *Workman and Hart* [2005]. Lead concentration in mantle melts is estimated

Table 3. End-Member Compositions of the Sources Used in the Mass-Balance Model

	Pb (ppm)	$^{206}Pb/^{204}Pb$	$^{207}Pb/^{204}Pb$	$^{207}Pb/^{204}Pb$	Reference for Pb Concentration	Reference for Pb Isotope Ratios
Depleted mantle	0.18	18.10	15.46	37.50	*Workman-Hart* [2005]; DMM composition, 10% partial melting with total mobilization of Pb	*Harpp-White*, [2001]; DUM component
Slab component	22	19.83	15.64	39.53	*White* [1993]; Floreana samples average composition $D_{liq/sol} = 10$ considered	*White* [1993]; Floreana samples average composition
Lower Crust	2.8	19.26	15.73	39.13	*Rudnick-Fountain* [1995]; estimate for continental arcs	*Weber et al*., [2002]; extreme isotopic composition of Colombian xenoliths (sample GRL-1)
Upper Crust	13	18.97	15.71	38.89	*Rudnick-Gao* [2003]; total crust composition	*Rudnick-Goldstein* [1990] and *Paul et al.* [2003]

assuming 10% partial melting and strong partitioning of Pb into melt (i.e., $D^{l/s} \gg 1$). Most of the subducted slab beneath Ecuador consists of the Carnegie ridge underlain by the Nazca plate oceanic crust and lithospheric mantle. The amount of sediments entering the subduction zone is likely very small and can be neglected. The Carnegie ridge consists of products emitted by the Galapagos hot spot. Its composition is explained by mixing four components according to *Harpp and White* [2001], whose extreme end-members are represented by the "unaffected" depleted mantle (DUM) and the enriched FLO component, corresponding to Floreana Island samples. We choose the enriched end-member signature (Floreana Island, *White et al*. [1993]) as representative of the slab component end-member. Lead concentration in slab fluids is inferred from the partitioning experiments of *Kessel et al*. [2005]. At 4 GPa, the partition coefficient of Pb between fluid and slab varies between 3.2 at 700°C and 19 at 800°C. In the absence of constraints on slab temperature variation across and along the arc, a unique intermediate value of 10 is used.

For lower crust, we take the most radiogenic composition of the Columbian xenoliths [*Weber et al*., 2002], which are the best representative of the Ecuadorian lower crust, and the Pb concentration of lower crust estimated by *Rudnick and Fountain* [1995] for continental arcs. The upper crust in Ecuador is extremely heterogeneous, and its average composition poorly constrained. We thus use the global average estimated by *Rudnick and Goldstein* [1990] (with $^{208}Pb/^{206}Pb$ ratio determined by *Paul et al.* [2003]) and the Pb concentration of total crust from *Rudnick and Gao* [2003]. Note that the average continental crust plots roughly at the unradiogenic end of Ecuadorian upper crust compositional range while Columbian xenoliths plot at the radiogenic end.

7.2. Geographical Distribution of Sources Imprint

Figure 13 displays component fractions against the distance from the trench. First of all, mantle melts largely dominate (mass fraction >70%) the Pb budget of Ecuadorian magmas. Mantle melts influence is greater in the frontal part of the arc and in the back arc (mass fraction >90%) than in the main arc (between 70% and 90% in mass). Conversely, lower crust assimilation increases away from the trench, from 3% in the Pilavo volcano up to 27% in Tungurahua, with a minimum of 10% in the main arc, but is low in the back arc (less than 5–6%). Upper crust assimilation plays a minor role compared to lower crust but nevertheless reaches 1–2.4% in the main arc and back-arc edifices. We notice that back-arc magmas are amongst the least contaminated by lower crust but bear upper crustal imprint. Lastly, slab component imprint is maximum (∼1%) along the frontal part of the arc and decreases away from the trench.

Figure 14 confirms that lower crust assimilation increases continuously from north to south in the frontal part of the arc while slab contribution decreases. Such a pattern is also observed along the Eastern Cordillera. However, Reventador and Sangay generally plot outside the trends of the Eastern Cordillera. The two volcanoes have the highest upper crust (>2%) and lowest slab (<0.25%) imprints of the Eastern Cordillera. Sangay, the southernmost volcano, is little contaminated by lower crust (13%) and has a strong mantle imprint (80%). Anomalously high slab contributions are recorded at Conos de Puyo and Puñalica, which could be linked to their peculiar location: those volcanic edifices lie upon the projected Grijalva Fracture Zone where tear could enhance slab melting as suggested by *Yogodzinski et al*. [2001] for the Kamchatka arc.

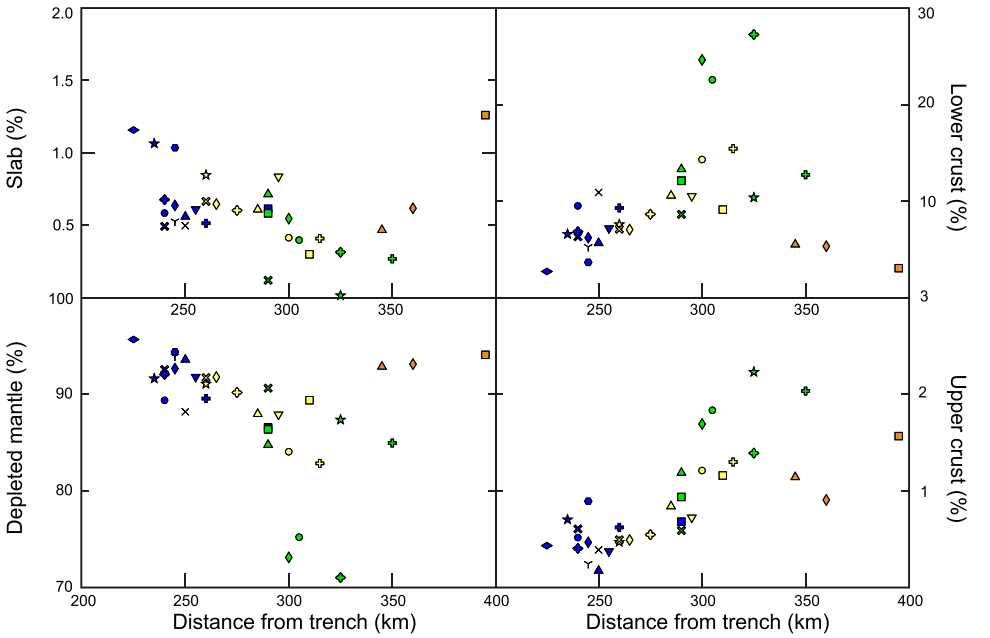

Figure 13. Mass-balance model. The mass fractions of upper crust, lower crust, mantle melts, and slab component at each volcanic center are plotted against distance from trench. Legend as in Figures 3 and 10.

In summary, based on the mass-balance model presented here, the mantle wedge is, by far, the major component of the magmas erupted in the Ecuadorian arc. Continental crust assimilation plays a key role, especially far from the trench, with the Eastern Cordillera volcanoes assimilating up to 27% of lower crust. In the frontal part of the arc, our model confirms that slab influence decreases from North to South while lower crust assimilation increases.

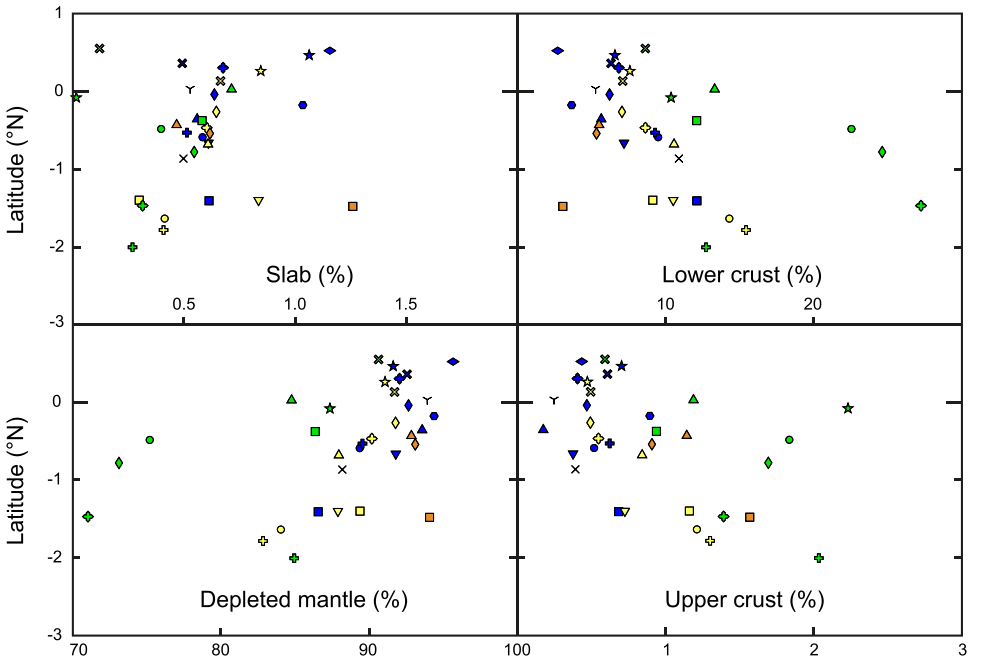

Figure 14. Mass-balance model. Component mass fractions plotted against latitude. Legend as in Figures 3 and 10.

8. Conclusion

This work filled in local gaps in data and allowed us to establish a detailed map of the geographical distribution of isotopic signatures in the Quaternary Ecuadorian arc. Our new data allowed us to discriminate between Western Cordillera, Eastern Cordillera and back-arc volcanic eruptive products based on lead isotopes. We confirmed the conclusions of previous across-arc studies regarding the decrease of slab input and mantle melting away from the trench, and the early dehydration of the slab beneath the frontal part of the arc. We estimated the various contributions of the mantle wedge, the slab component and the upper and lower crust in Ecuadorian volcanism. Crustal contamination is dominated by lower crust assimilation, which is maximal in the main arc (from 10% to 27%). Our model also confirms the decreasing contribution of slab component on magma geochemistry away from the trench. Along-arc variations in trace element ratios and isotopes were also identified, especially in the frontal part of the arc which shows two major trends: (1) antithetic variations of $^{207}Pb/^{204}Pb$ and $^{143}Nd/^{144}Nd$ record an increase in crustal contamination of magma southwards, confirmed by the quantitative model; and (2) increase in $^{206}Pb/^{204}Pb$ and decrease in Ba/Th north and south to 0.5°S reflects a change in subducting slab inputs, with the aqueous fluid/siliceous melt ratio decreasing away from 0.5°S. Slab melting might be linked to the decreasing age of the oceanic floor toward the north while decreasing influence of the slab to the south may be due to the subduction of an older and colder oceanic crust south of the Grijalva Fault Zone. Along-arc isotopic variations might also record the geometry of the subducting slab, whose flexure induces a change in the thickness of the mantle wedge beneath the volcanic arc, and thus, affects the dilution of the slab input into the mantle wedge.

Acknowledgments

The complete data set (new analyses and unpublished IRD/IGEPN data) is available online as supporting information. This work benefited from the financial support from the French Government Laboratory of Excellence initiative ANR-10-LABX-0006, the Région Auvergne and the European Regional Development Funds. It is also part of an Ecuadorian-French cooperation programme carried out between the Instituto Geofísico, Escuela Politécnica Nacional (IGEPN), Quito, Ecuador and the French Institut de Recherche pour le Développement (IRD): the Laboratoire Mixte International "Séismes et Volcans dans les Andes du Nord." We thank Chantal Bosq, Jean-Luc Piro, Marie-Laure Rouget, Delphine Auclair and Mhammed Benbakkar for providing analytical support and Fran van Wyk de Vries for the English improvement of this manuscript. We also thank the editor Janne Blichert-Toft for handling this paper and the three reviewers (Dennis Geist, Kenneth W.W. Sims, and an anonymous reviewer) whose advice significantly improved the quality of this manuscript. This is Laboratory of Excellence ClerVolc contribution number 243.

References

Annen, C., J. D. Blundy, and R. S. J. Sparks (2006), The genesis of intermediate and silicic magmas in deep crustal hot zones, *J. Petrol.*, *47*(3), 505–539, doi:10.1093/petrology/egi084.

Aspden, J. A., and M. Litherland (1992), The geology and Mesozoic collisional history of the Cordillera Real, Ecuador, *Tectonophysics*, *205*(1–3), 187–204, doi:10.1016/0040-1951(92)90426-7.

Baby, P., M. Rivadeneria, and R. Barragan (2004), *La Cuenca Oriente: Geología y Petróleo*, Travaux de l'Institut Français d'Etudes Andines, vol. 144, 414 pp.

Barazangi, M., and B. L. Isacks (1976), Subduction of the Nazca plate beneath Peru: Evidence from spatial distribution of earthquakes, *Geology*, *4*, 686–692, doi:10.1111/j.1365-246X.1979.tb06778.x.

Barberi, F., M. Coltelli, G. Ferrara, F. Innocenti, J. M. Navarro, and R. Santacroce (1988), Plio-Quaternary volcanism in Ecuador, *Geol. Mag.*, *125*(1), 1–14.

Barragan, R., D. Geist, M. L. Hall, P. Larson, and M. Kurz (1998), Subduction controls on the compositions of lavas from the Ecuadorian Andes, *Earth Planet. Sci. Lett.*, *154*, 153–166, doi:10.1016/S0012-821X(97)00141-6.

Barrat, J. W., F. Keller, J. Amossé, R. N. Taylor, R. W. Nesbitt, and T. Hirata (1996), Determination of rare earth elements in sixteen silicate reference samples by Icp-Ms After Tm addition and ion exchange separation, *Geostand. Newslett.*, *20*(1), 133–139, doi:10.1111/j.1751-908X.1996.tb00177.x.

Bernard, B., and D. Andrade (2011), Volcanes Cuaternarios del Ecuador Continental, Instituto Geofísico - Escuela Politécnica Nacional and Institut de Recherche pour le Développement, Poster Informativo.

Bès de Berc, S., J. C. Soula, P. Baby, M. Souris, F. Christophoul, and J. Rosero (2005), Geomorphic evidence of active deformation and uplift in a modern continental wedge-top—Foredeep transition: Example of the eastern Ecuadorian Andes, *Tectonophysics*, *399*(1–4), 351–380, doi:10.1016/j.tecto.2004.12.030.

Bourdon, E., J.-P. Eissen, M.-A. Gutscher, M. Monzier, P. Samaniego, C. Robin, C. Bollinger, and J. Cotten (2002a), Slab melting and slab melt metasomatism in the Northern Andean Volcanic Zone: Adakites and high-Mg andesites from Pichincha volcano (Ecuador), *Bull. Soc. Geol. France*, *173*(3), 195–206.

Bourdon, E., J.-P. Eissen, M. Monzier, C. Robin, H. Martin, J. Cotten, and M. L. Hall (2002b), Adakite-like lavas from Antisana Volcano (Ecuador): Evidence for slab melt metasomatism beneath Andean Northern Volcanic Zone, *J. Petrol.*, *43*(2), 199–217. [Available at http://petrology.oxfordjournals.org/content/43/2/199.short.]

Bourdon, E., J.-P. Eissen, M.-A. Gutscher, M. Monzier, M. L. Hall, and J. Cotten (2003), Magmatic response to early aseismic ridge subduction: The Ecuadorian margin case (South America), *Earth Planet. Sci. Lett.*, *205*(3–4), 123–138.

Bryant, J. A., G. M. Yogodzinski, M. L. Hall, J. L. Lewicki, and D. G. Bailey (2006), Geochemical constraints on the origin of volcanic rocks from the Andean Northern volcanic zone, Ecuador, *J. Petrol.*, *47*(6), 1147–1175, doi:10.1093/petrology/egl006.

Chiaradia, M. (2009), Adakite-like magmas from fractional crystallization and melting-assimilation of mafic lower crust (Eocene Macuchi arc, Western Cordillera, Ecuador), *Chem. Geol.*, *265*(3–4), 468–487, doi:10.1016/j.chemgeo.2009.05.014.

Chiaradia, M., L. Fontboté, and A. Paladines (2004), Metal sources in mineral deposits and crustal rocks of Ecuador (1°N–4°S): A lead isotope synthesis, *Econ. Geol.*, *99*(6), 1085–1106, doi:10.2113/gsecongeo.99.6.1085.

Chiaradia, M., O. Müntener, B. Beate, and D. Fontignie (2009), Adakite-like volcanism of Ecuador: Lower crust magmatic evolution and recycling, *Contrib. Mineral. Petrol.*, *158*(5), 563–588, doi:10.1007/s00410-009-0397-2.

Chiaradia, M., O. Müntener, and B. Beate (2011), Enriched basaltic andesites from mid-crustal fractional crystallization, recharge, and assimilation (Pilavo volcano, Western Cordillera of Ecuador), *J. Petrol.*, *52*(6), 1107–1141, doi:10.1093/petrology/egr020.

Cotten, J., A. Le Dez, M. Bau, M. Caroff, R. C. Maury, P. Dulski, S. Fourcaden, M. Bohn, and R. Brousse (1995), Origin of anomalous rare-earth element and yttrium enrichments in subaerially exposed basalts: Evidence from French Polynesia, *Chem. Geol.*, *119*(1–4), 115–138, doi:10.1016/0009-2541(94)00102-E.

Davidson, J. P., and S. L. De Silva (1992), Volcanic rocks from the Bolivian Altiplano: Insights into crustal structure, contamination, and magma genesis in the Central Andes, *Geology*, *20*(12), 1127–1130, doi:10.1130/0091-7613(1992)020<1127:VRFTBA>2.3.CO;2.
Davidson, J. P., and S. L. De Silva (1995), Late Cenozoic magmatism of the Bolivian Altiplano, *Contrib. Mineral. Petrol.*, *119*, 387–408, doi:10.1007/BF00286937.
Defant, M., and M. Drummond (1990), Derivation of some modern arc magmas by melting of young subducted lithosphere, *Nature*, *347*, 662–665.
Delacour, A., M. C. Gerbe, J. C. Thouret, G. Wörner, and P. Paquereau-Lebti (2007), Magma evolution of Quaternary minor volcanic centres in southern Peru, Central Andes, *Bull. Volcanol.*, *69*(6), 581–608, doi:10.1007/s00445-006-0096-z.
Dickinson, W. R. (1975), Potash-Depth (K-h) relations in continental margin and intra-oceanic magmatic arcs, *Geology*, *3*(2), 53–56, doi:10.1130/0091-7613(1975)3<53:PKRICM>2.0.CO;2.
Droux, A., and M. Delaloye (1996), Petrography and geochemistry of Plio-Quaternary calc-alkaline volcanoes of Southwestern Colombia, *J. South Am. Earth Sci.*, *9*(1–2), 27–41, doi:10.1016/0895-9811(96)00025-9.
Elliott, T., T. Plank, A. Zindler, W. M. White, and B. Bourdon (1997), Element transport from slab to volcanic front at the Mariana Arc, *J. Geophys. Res.*, *102*(B7), 14,991–15,019.
Feeley, T. C., and J. P. Davidson (1994), Petrology of calc-alkaline lavas at volcan ollagüe and the origin of compositional diversity at central andean stratovolcanoes, *J. Petrol.*, *35*(5), 1295–1340, doi:10.1093/petrology/35.5.1295.
Feininger, T., and M. K. Seguin (1983), Simple Bouguer gravity anomaly field and the inferred crustal structure of continental Ecuador, *Geology*, *11*(1), 40–44, doi:10.1130/0091-7613(1983)11<40:SBGAFA>2.0.CO;2.
Garrison, J. M., and J. P. Davidson (2003), Dubious case for slab melting in the Northern volcanic zone of the Andes, *Geology*, *31*(6), 565–568, doi:10.1130/0091-7613(2003)031<0565:DCFSMI>2.0.CO;2.
Garrison, J., J. Davidson, M. Reid, and S. Turner (2006), Source versus differentiation controls on U-series disequilibria: Insights from Cotopaxi Volcano, Ecuador, *Earth Planet. Sci. Lett.*, *244*(3–4), 548–565, doi:10.1016/j.epsl.2006.02.013.
Garrison, J. M., J. P. Davidson, M. L. Hall, and P. Mothes (2011), Geochemistry and petrology of the most recent deposits from Cotopaxi Volcano, Northern Volcanic Zone, Ecuador, *J. Petrol.*, *52*(9), 1641–1678, doi:10.1093/petrology/egr023.
Gazel, E., et al. (2015), Continental crust generated in oceanic arcs, *Nat. Geosci*, *8*(4), 321–327, doi:10.1038/ngeo2392.
Grove, T., S. Parman, S. Bowring, R. Price, and M. Baker (2002), The role of an H_2O-rich fluid component in the generation of primitive basaltic andesites and andesites from the Mt. Shasta region, N California, *Contrib. Mineral. Petrol.*, *142*(4), 375–396, doi:10.1007/s004100100299.
Guillier, B., J.-L. Chatelain, É. Jaillard, H. Yepes, G. Poupinet, and J.-F. Fels (2001), Seismological evidence on the geometry of the orogenic system in central-northern Ecuador (South America), *Geophys. Res. Lett.*, *28*(19), 3749–3752.
Gutscher, M.-A., J. Malavieille, S. Lallemand, and J. Y. Collot (1999), Tectonic segmentation of the North Andean margin: Impact of the Carnegie Ridge collision, *Earth Planet. Sci. Lett.*, *168*(3–4), 255–270, doi:10.1016/S0012-821X(99)00060-6.
Hall, M. L., and C. A. Wood (1985), Volcano-tectonic segmentation of the northern Andes Volcano-tectonic segmentation of the northern Andes, *Geology*, *13*, 203–207, doi:10.1130/0091-7613(1985)13<203.
Hall, M. L., P. Samaniego, J.-L. Le Pennec, and J. B. Johnson (2008), Ecuadorian Andes volcanism: A review of Late Pliocene to present activity, *J. Volcanol. Geotherm. Res.*, *176*(1), 1–6, doi:10.1016/j.jvolgeores.2008.06.012.
Hanyu, T., et al. (2012), Across- and along-arc geochemical variations of lava chemistry in the Sangihe arc: Various fluid and melt slab fluxes in response to slab temperature, *Geochem. Geophys. Geosyst.*, *13*, Q10021, doi:10.1029/2012GC004346.
Harpp, K. S., and W. M. White (2001), Tracing a mantle plume: Isotopic and trace element variations of Gala´pagos seamounts, *Geochem. Geophys. Geosyst.*, *2*(6), 1042, doi:10.1029/2000GC00013.
Heydolph, K., K. Hoernle, F. Hauff, P. Van den Bogaard, M. Portnyagin, I. Bindeman, and D. Garbe-Schönberg (2012), Along and across arc geochemical variations in NW Central America: Evidence for involvement of lithospheric pyroxenite, *Geochim. Cosmochim. Acta*, *84*, 459–491, doi:10.1016/j.gca.2012.01.035.
Hickey-Vargas, R., S. Holbik, D. Tormey, F. A. Frey, and R. H. Moreno Roa (2016), Basaltic rocks from the Andean Southern Volcanic Zone: Insights from the comparison of along-strike and small-scale geochemical variations and their sources, *Lithos*, *258–259*, 115–132, doi:10.1016/j.lithos.2016.04.014.
Hidalgo, S., M. Monzier, H. Martin, G. Chazot, J.-P. Eissen, and J. Cotten (2007), Adakitic magmas in the Ecuadorian Volcanic Front: Petrogenesis of the Iliniza Volcanic Complex (Ecuador), *J. Volcanol. Geotherm. Res.*, *159*(4), 366–392, doi:10.1016/j.jvolgeores.2006.07.007.
Hidalgo, S., M. C. Gerbe, H. Martin, P. Samaniego, and E. Bourdon (2012), Role of crustal and slab components in the Northern Volcanic Zone of the Andes (Ecuador) constrained by Sr–Nd–O isotopes, *Lithos*, *132–133*, 180–192, doi:10.1016/j.lithos.2011.11.019.
Hildreth, W., and S. Moorbath (1988), Crustal contributions to arc magmatism in the Andes of Central Chile, *Contrib. Mineral. Petrol.*, *98*(4), 455–489, doi:10.1007/BF00372365.
Hoffer, G., J.-P. Eissen, B. Beate, E. Bourdon, M. Fornari, and J. Cotten (2008), Geochemical and petrological constraints on rear-arc magma genesis processes in Ecuador: The Puyo cones and Mera lavas volcanic formations, *J. Volcanol. Geotherm. Res.*, *176*(1), 107–118, doi:10.1016/j.jvolgeores.2008.05.023.
Hofmann, A. W. (1997), Mantle geochemistry: The message from oceanic volcanism, *Nature*, *385*, 219–229.
Hora, J. M., B. S. Singer, and G. Wörner (2007), Volcano evolution and eruptive flux on the thick crust of the Andean Central Volcanic Zone: 40Ar/39Ar constraints from Volcán Parinacota, Chile, *Bull. Geol. Soc. Am.*, *119*(3–4), 343–362, doi:10.1130/B25954.1.
Hughes, R. A., and L. F. Pilatasig (2002), Cretaceous and tertiary terrane accretion in the Cordillera Occidental of the Andes of Ecuador, *Tectonophysics*, *345*(1–4), 29–48, doi:10.1016/S0040-1951(01)00205-0.
Ishizuka, O., R. N. Taylor, M. Yuasa, J. A. Milton, R. W. Nesbitt, K. Uto, and I. Sakamoto (2007), Processes controlling along-arc isotopic variation of the southern Izu-Bonin arc, *Geochem. Geophys. Geosyst.*, *8*, Q06008, doi:10.1029/2006GC001475.
Jaillard, É., P. Bengtson, M. Ordoñez, W. Vaca, A. Dhondt, J. Suárez, and J. Toro (2008), Sedimentary record of terminal Cretaceous accretions in Ecuador: The Yunguilla Group in the Cuenca area, *J. South Am. Earth Sci.*, *25*(2), 133–144, doi:10.1016/j.jsames.2007.08.002.
Kelemen, P. B., G. M. Yogodzinski, and D. W. Scholl (2003), Along-strike variation in the Aleutian Island Arc: Genesis of high Mg# andesite and implications for continental crust, *Geophys. Monogr.*, *138*, 223–276, doi:10.1029/138GM11.
Kelemen, P. B., K. Hanghoj, and A. R. Greene (2014), One view of the geochemistry of subduction-related magmatic arcs, with an emphasis on primitive andesite and lower crust, *Treat. Geochem.*, *4*, 749–806, doi:10.1016/B978-0-08-095975-7.00323-5.
Kelley, K. A., T. Plank, L. Farr, J. Ludden, and H. Staudigel (2005), Subduction cycling of U, Th, and Pb, *Earth Planet. Sci. Lett.*, *234*, 369–383, doi:10.1016/j.epsl.2005.03.005.
Kendrick, E., M. Bevis, R. Smalley, B. Brooks, R. B. Vargas, E. Lauría, and L. P. S. Fortes (2003), The Nazca-South America Euler vector and its rate of change, *J. South Am. Earth Sci.*, *16*(2), 125–131, doi:10.1016/S0895-9811(03)00028-2.

Kessel, R., M. W. Schmidt, P. Ulmer, and T. Pettke (2005), Trace element signature of subduction-zone fluids, melts and supercritical liquids at 120–180 km depth, *Nature*, *437*, 724–727, doi:10.1038/nature03971.

Le Voyer, M., E. F. Rose-Koga, M. Laubier, and P. Schiano (2008), Petrogenesis of arc lavas from the rucu pichincha and pan de azucar volcanoes (Ecuadorian arc): Major, trace element, and boron isotope evidences from olivine-hosted melt inclusions, *Geochem. Geophys. Geosyst.*, *9*, Q12027, doi:10.1029/2008GC002173.

Lonsdale, P. (2005), Creation of the Cocos and Nazca plates by fission of the Farallon plate, *Tectonophysics*, *404*(3–4), 237–264, doi:10.1016/j.tecto.2005.05.011.

Luzieux, L. D. A., F. Heller, R. A. Spikings, C. F. Vallejo, and W. Winkler (2006), Origin and Cretaceous tectonic history of the coastal Ecuadorian forearc between 1°N and 3°S: Paleomagnetic, radiometric and fossil evidence, *Earth Planet. Sci. Lett.*, *249*(3–4), 400–414, doi:10.1016/j.epsl.2006.07.008.

Mamani, M., A. Tassara, and G. Wörner (2008), Composition and structural control of crustal domains in the central Andes, *Geochem. Geophys. Geosyst.*, *9*, Q03006, doi:10.1029/2007GC001925.

Mamani, M., G. Wörner, and T. Sempere (2010), Geochemical variations in igneous rocks of the Central Andean orocline (13°S to 18°S): Tracing crustal thickening and magma generation through time and space, *Bull. Geol. Soc. Am.*, *122*(1–2), 162–182, doi:10.1130/B26538.1.

Martin, H., J. F. Moyen, M. Guitreau, J. Blichert-Toft, and J.-L. Le Pennec (2014), Why Archaean TTG cannot be generated by MORB melting in subduction zones, *Lithos*, *198–199*(1), 1–13, doi:10.1016/j.lithos.2014.02.017.

Michaud, F., C. Witt, and J.-Y. Royer (2009), Influence of the subduction of the Carnegie volcanic ridge on Ecuadorian geology: Reality and fiction, *Geol. Soc. Am. Mem.*, *204*(10), 217–228, doi:10.1130/2009.1204(10).

Monzier, M., C. Robin, J.-P. Eissen, and J. Cotten (1997), Geochemistry vs. seismo-tectonics along the volcanic New Hebrides Central Chain (Southwest Pacific), *J. Volcanol. Geotherm. Res.*, *78*(1–2), 1–29, doi:10.1016/S0377-0273(97)00006-1.

Monzier, M., C. Robin, P. Samaniego, M. L. Hall, J. Cotten, P. Mothes, and N. Arnaud (1999), Sangay volcano, Ecuador: Structural development, present activity and petrology, *J. Volcanol. Geotherm. Res.*, *90*(1–2), 49–79, doi:10.1016/S0377-0273(99)00021-9.

Paul, D., W. M. White, and D. L. Turcotte (2003), Constraints on the 232 Th//238U ratio (K) of the continental crust, *Geochem. Geophys. Geosyst.*, *4*(12), 1102, doi:10.1029/2002GC000497.

Peacock, S. M., T. Rushmer, and A. B. Thompson (1994), Partial melting of subducting oceanic crust, *Earth Planet. Sci. Lett.*, *121*(1–2), 227–244, doi:10.1016/0012-821X(94)90042-6.

Pedoja, K., J. F. Dumont, M. Lamothe, L. Ortlieb, J. Y. Collot, B. Ghaleb, M. Auclair, V. Alvarez, and B. Labrousse (2006), Plio-Quaternary uplift of the Manta Peninsula and La Plata Island and the subduction of the Carnegie Ridge, central coast of Ecuador, *J. South Am. Earth Sci.*, *22*(1–2), 1–21, doi:10.1016/j.jsames.2006.08.003.

Pennington, W. D. (1981), Subduction of the Eastern Panama basin and seismotectonics of the Northwestern South America, *J. Geophys. Res.*, *86*(B11), 10,753–10,770.

Pin, C., and J. F. Santos Zalduegui (1997), Sequential separation of light rare-earth elements, thorium and uranium by miniaturized extraction chromatography: Application to isotopic analyses of silicate rocks, *Anal. Chim. Acta*, *339*, 79–89.

Pin, C., D. Briot, C. Bassin, and F. Poitrasson (1994), Concomitant separation of strontium and samarium-neodymium for isotopic analysis in silicate samples, based on specific extraction chromatography, *Anal. Chim. Acta*, *298*, 209–217.

Proust, J. N., C. Martillo, F. Michaud, J. Y. Collot, and O. Dauteuil (2016), Subduction of seafloor asperities revealed by a detailed stratigraphic analysis of the active margin shelf sediments of Central Ecuador, *Mar. Geol.*, *380*, 345–362, doi:10.1016/j.margeo.2016.03.014.

Reynaud, C., E. Jaillard, H. Lapierre, M. Mamberti, and G. H. Mascle (1999), Oceanic plateau and island arcs of southwestern Ecuador: Their place in the geodynamic evolution of northwestern South America, *Tectonophysics*, *307*, 235–254, doi:10.1016/S0040-1951(99)00099-2.

Robin, C., P. Samaniego, J.-L. Le Pennec, P. Mothes, and J. Van der Plicht (2008), Late Holocene phases of dome growth and Plinian activity at Guagua Pichincha volcano (Ecuador), *J. Volcanol. Geotherm. Res.*, *176*(1), 7–15, doi:10.1016/j.jvolgeores.2007.10.008.

Robin, C., J.-P. Eissen, P. Samaniego, H. Martin, M. L. Hall, and J. Cotten (2009), Evolution of the late Pleistocene Mojanda-Fuya Fuya volcanic complex (Ecuador), by progressive adakitic involvement in mantle magma sources, *Bull. Volcanol.*, *71*(3), 233–258, doi:10.1007/s00445-008-0219-9.

Rudnick, R. L., and S. L. Goldstein (1990), The Pb isotopic compositions of lower crustal xenoliths and the evolution of lower crustal Pb, *Earth Planet. Sci. Lett.*, *98*, 192–207.

Rudnick, R. L., and D. M. Fountain (1995), Nature and composition of the continental crust: A lower crustal perspective, *Rev. Geophys.*, *33*(3), 267–309.

Rudnick, R. L., and S. Gao (2003), Composition of the continental crust, *Treat. Geochem.*, *3*, 1–64, doi:10.1016/B0-08-043751-6/03016-4.

Ryan, J. G., J. Morris, F. Tera, W. P. Leeman, and A. Tsvetkov (1995), Cross-arc geochemical variations in the Kurile Arc as a function of slab depth, *Science*, *270*(5236), 625–627, doi:10.1126/science.270.5236.625.

Sallarès, V., P. Charvis, E. R. Flueh, and J. Bialas (2003), Seismic structure of Cocos and Malpelo Volcanic Ridges and implications for hot spot-ridge interaction, *J. Geophys. Res.*, *108*(B12), 1–21, doi:10.1029/2003JB002431.

Samaniego, P., H. Martin, M. Monzier, C. Robin, M. Fornari, J.-P. Eissen, and J. Cotten (2005), Temporal evolution of magmatism in the Northern Volcanic Zone of the Andes: The geology and petrology of cayambe volcanic complex (Ecuador), *J. Petrol.*, *46*(11), 2225–2252, doi:10.1093/petrology/egi053.

Samaniego, P., J. P. Eissen, J. L. Le Pennec, C. Robin, M. L. Hall, P. Mothes, D. Chavrit, and J. Cotten (2008), Pre-eruptive physical conditions of El Reventador volcano (Ecuador) inferred from the petrology of the 2002 and 2004-05 eruptions, *J. Volcanol. Geotherm. Res.*, *176*(1), 82–93, doi:10.1016/j.jvolgeores.2008.03.004.

Samaniego, P., C. Robin, G. Chazot, E. Bourdon, and J. Cotten (2010), Evolving metasomatic agent in the Northern Andean subduction zone, deduced from magma composition of the long-lived Pichincha volcanic complex (Ecuador), *Contrib. Mineral. Petrol.*, *160*(2), 239–260, doi:10.1007/s00410-009-0475-5.

Samaniego, P., J.-L. Le Pennec, C. Robin, and S. Hidalgo (2011), Petrological analysis of the pre-eruptive magmatic process prior to the 2006 explosive eruptions at Tungurahua volcano (Ecuador), *J. Volcanol. Geotherm. Res.*, *199*(1–2), 69–84, doi:10.1016/j.jvolgeores.2010.10.010.

Samaniego, P., D. Barba, C. Robin, M. Fornari, and B. Bernard (2012), Eruptive history of Chimborazo volcano (Ecuador): A large, ice-capped and hazardous compound volcano in the Northern Andes, *J. Volcanol. Geotherm. Res.*, *221–222*, 33–51, doi:10.1016/j.jvolgeores.2012.01.014.

Schiano, P., M. Monzier, J.-P. Eissen, H. Martin, and K. T. Koga (2010), Simple mixing as the major control of the evolution of volcanic suites in the Ecuadorian Andes, *Contrib. Mineral. Petrol.*, *160*(2), 297–312, doi:10.1007/s00410-009-0478-2.

Sørensen, E. V., and P. M. Holm (2008), Petrological inferences on the evolution of magmas erupted in the Andagua Valley, Peru (Central Volcanic Zone), *J. Volcanol. Geotherm. Res.*, *177*(2), 378–396, doi:10.1016/j.jvolgeores.2008.05.021.

Spandler, C., and C. Pirard (2013), Element recycling from subducting slabs to arc crust: A review, *Lithos*, *170–171*, 208–223, doi:10.1016/j.lithos.2013.02.016.

Spikings, R. A., W. Winkler, D. Seward, and R. Handler (2001), Along-strike variations in the thermal and tectonic response of the continental Ecuadorian Andes to the collision with heterogeneous oceanic crust, *Earth Planet. Sci. Lett.*, *186*(1), 57–73, doi:10.1016/S0012-821X(01)00225-4.

Stolper, E., and S. Newman (1994), The role of water in the petrogenesis of Mariana trough magmas, *Earth Planet. Sci. Letters*, *121*, 293–325, doi:10.1016/0012-821X(94)90074-4.

Syracuse, E. M., P. E. Van Keken, G. A. Abers, D. Suetsugu, C. Bina, T. Inoue, D. Wiens, and M. Jellinek (2010), The global range of subduction zone thermal models, *Phys. Earth Planet. Inter.*, *183*(1–2), 73–90, doi:10.1016/j.pepi.2010.02.004.

Taylor, S., and S. McLennan (1995), The geochemical evolution of the continental crust, *Rev. Geophys.*, *33*(2), 241–265, doi:10.1029/95RG00262.

Todt, W., R. Cliff, A. Hanser, and A. Hofmann (1996), Evaluation of a 202Pb–205Pb double spike for high-precision lead isotope analysis, *Geophys. Monogr. Ser.*, *95*(October 2015), 429–437, doi:10.1029/GM095p0429.

Turner, S. J., C. H. Langmuir, R. F. Katz, M. A. Dungan, and S. Escrig (2016), Parental arc magma compositions dominantly controlled by mantle-wedge thermal structure, *Nat. Geosci.*, *1*(August), 1–6, doi:10.1038/NGEO2788.

Vlastélic I., and L. Dosso (2005), Initiation of a plume-ridge interaction in the South Pacific recorded by high-precision Pb isotopes along Hollister Ridge, *Geochem. Geophys. Geosyst.*, *6*, Q05011, doi:1029/2004GC000902.

Vlastélic, I., T. Staudacher, C. Deniel, J. L. Devidal, B. Devouard, A. Finizola, and P. Télouk (2013), Lead isotopes behavior in the fumarolic environment of the Piton de la Fournaise volcano (Réunion Island), *Geochim. Cosmochim. Acta*, *100*, 297–314, doi:10.1016/j.gca.2012.09.016.

Weber, M. B. I., J. Tarney, P. D. Kempton, and R. W. Kent (2002), Crustal make-up of the northern Andes: Evidence based on deep crustal xenolith suites, Mercaderes, SW Colombia, *Tectonophysics*, *345*, 49–82, doi:10.1016/S0040-1951(01)00206-2.

Wedepohl, K. H. (1995), The composition of the continental crust, *Geochim. Cosmochim. Acta*, *59*(7), 1217–1232, doi:10.1016/0016-7037(95)00038-2.

Werner, R., K. Hoernle, U. Barckhausen, and F. Hauff (2003), Geodynamic evolution of the Galapagos hot spot system (Central East Pacific) over the past 20 m.y.: Constraints from morphology, geochemistry, and magnetic anomalies, *Geochem. Geophys. Geosyst.*, *4*(12), doi:10.1029/2003GC000576.

White, W. M., A. R. McBirney, and R. A. Duncan (1993), Petrology and geochemistry of the Galapagos Islands: Portait of a pathological mantle plume, *J. Geophys. Res.*, *98*(B11), 19,533–19,563.

Workman, R. K., and S. R. Hart (2005), Major and trace element composition of the depleted MORB mantle (DMM), *Earth Planet. Sci. Lett.*, *231*(1–2), 53–72, doi:10.1016/j.epsl.2004.12.005.

Yepes, H., L. Audin, A. Alvarado, C. Beauval, J. Aguilar, Y. Font, and F. Cotton (2016), A new view for the geodynamics of Ecuador: Implication in seismogenic source definition and seismic hazard assessment, *Tectonics*, *35*(5), 1249–1279, doi:10.1002/2015TC003941.

Yogodzinski, G. M., J. M. Lees, T. G. Churikova, F. Dorendorf, G. Wöerner, and O. N. Volynets (2001), Geochemical evidence for the melting of subducting oceanic lithosphere at plate edges, *Nature*, *409*, 500–504, doi:10.1038/35054039.

Yogodzinski, G. M., S. T. Brown, P. B. Kelemen, J. D. Vervoort, M. Portnyagin, K. W. W. Sims, K. Hoernle, B. R. Jicha, and R. Werner (2015), The role of subducted basalt in the source of Island Arc Magmas: Evidence from seafloor lavas of the Western Aleutians, *J. Petrol.*, *56*(3), 441–492, doi:10.1093/petrology/egv006.